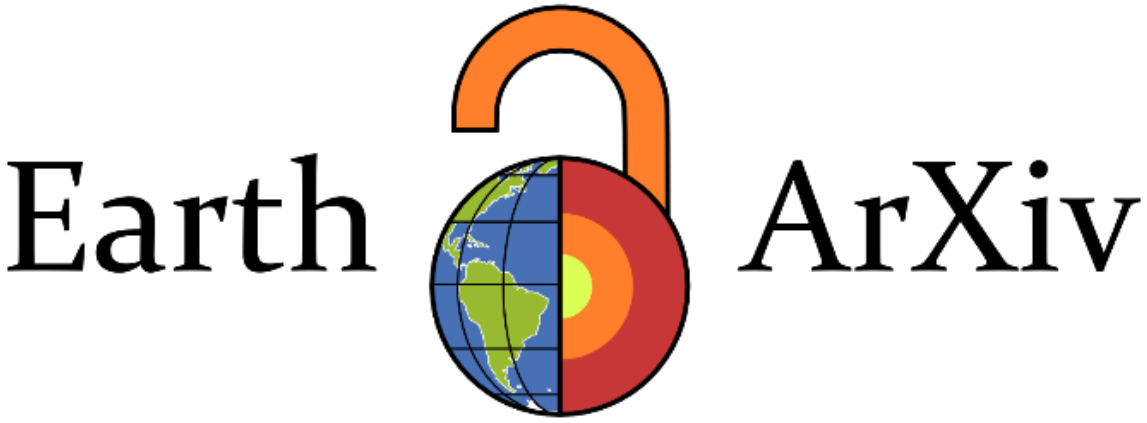

Vegetation Does Not Control Suspended Sediment Deposition in Salt Marshes

C. W. Lester[1,2], A. B. Murray[1], and Orencio Durán Vinent[3], Marco Marani[4], Andrea D'Alpaos[5], Sonia Silvestri[6], Tegan Blount[5], Zhicheng Yang[1]

[1]Division of Earth and Climate Sciences, Duke University, Durham, NC, USA
[2]Department of Physics and Physical Oceanography, University of North Carolina Wilmington, Wilmington, NC, USA
[3]Department of Ocean Engineering, Texas A&M University, College Station, TX, USA
[4]Department of Civil, Environmental, and Architectural Engineering, University of Padova, Padova, Italy
[5]Department of Geosciences, University of Padova, Padova, Italy
[6]Department of Biological, Geological and Environmental Sciences, University of Bologna, Padova, Italy

Key Points:

- Suspended sediment deposition on marsh platforms is independent of vegetation density
- Patterns of sediment deposition rates are set by marsh size, tidal characteristics, and grain settling rates
- Decoupling suspended sediment and vegetation deposition simplifies marsh evolution modeling

Corresponding author: Conner W. Lester, `conner.lester@duke.edu, lesterc@uncw.edu`

Abstract

Intertidal marshes are valuable geophysical systems, but their extent is rapidly declining globally. Marshes tend to keep up with sea-level rise through suspended-sediment and organic-matter deposition, up to a marsh-specific threshold rate of sea-level rise. Studies that explore marsh survival often assume that inorganic sediment deposition rates are directly linked to the density of marsh vegetation—coupling the inorganic and organic deposition processes. Here we examine the fluid-dynamics regulating sediment transport across a vegetated marsh and derive a framework for platform-wide sediment deposition. We demonstrate that sediment deposition rates are largely independent of vegetation density due to quasi-steady tidal propagation and vegetation-generated turbulence. Consequently, sediment deposition rates are primarily controlled by marsh size and tidal properties. Supported by extensive observations, these findings simplify modeling of long-term marsh dynamics by decoupling inorganic and organic deposition and offer insights into the processes that determine marsh resilience to accelerating sea-level rise.

Plain Language Summary

Salt marshes provide diverse coastal ecosystems and act as sinks of atmospheric carbon. Marshes are drowning as sea-level rise rates increase, making understanding their dynamics crucial. Marshes can build elevation and keep up with rising sea levels through both sediment deposition and the burial of plant material. Many studies assume that the amount of sediment settling on a marsh depends on how dense the vegetation is—coupling plant and sediment dynamics and adding complexity to marsh modeling. We show that this is not the case. Using theory and field data, we find that sediment deposition on marsh platforms depends mainly on local tidal properties, marsh size, and grain settling rates, and not on vegetation density. Vegetation is still essential because it stabilizes the surface and prevents erosion, but it does not control how much sediment settles. This understanding simplifies how we predict whether marshes can keep pace with sea level rise and helps improve forecasts of marsh evolution under climate change.

1 Introduction

Salt marshes are vital coastal ecosystems characterized by their rich biodiversity and significant role in carbon sequestration through the annual growth and burial of marsh vegetation (Campbell et al., 2022; Kirwan & Megonigal, 2013). Their ability to persist under sea-level rise has long been linked to the deposition of inorganic sediment supplied from tidal channels and the accumulation of organic matter from plant production across the marsh platform (Morris et al., 2002). This eco-geomorphodynamic framework emphasizes how vegetation growth and sediment deposition create internal feedbacks that set a marsh's equilibrium state (Marani et al., 2007; Morris et al., 2002). Within this view, marshes either accrete rapidly enough to keep pace with sea-level rise or drown once sea-level rise exceeds their capacity for net accretion (Marani et al., 2010; Kirwan et al., 2010). Understanding what governs sediment and organic deposition rates in marshes is therefore central to predicting their long-term stability.

Marsh platform elevations relative to mean sea level, $Z(x,t)$, evolve over multiple-year timescales according to $\partial_t Z = \bar{\varphi}_{\mathrm{inorg}} + \bar{\varphi}_{\mathrm{org}} - R$, where $\bar{\varphi}_{\mathrm{inorg}}$ and $\bar{\varphi}_{\mathrm{org}}$ are the time averaged accretion rates of suspended mineral sediment and organic matter, respectively, and R is the average rate of sea level rise. (On vegetated marsh platforms, erosion is typically considered negligible due to the reduced bed shear stress within vegetated canopies; see Supporting Information (SI) Section S1.5; Temmerman et al. (2007); Fagherazzi et al. (2020); Marani et al. (2007, 2010).) The organic deposition rate $\bar{\varphi}_{\mathrm{org}}$ represents primarily the burial of plant roots and is often expressed empirically as a function of elevation Z, encapsulating a suite of physiological and biogeochemical processes (Morris et al., 2002; Marani et al., 2013). In contrast, the deposition of suspended mineral sediment $\bar{\varphi}_{\mathrm{inorg}}$ is commonly assumed to depend on vegetation density (aboveground biomass), coupling the two deposition processes, $\bar{\varphi}_{\mathrm{inorg}} \rightleftharpoons \bar{\varphi}_{\mathrm{org}}$ (Kirwan & Murray, 2007; Zhang et al., 2020; Marani et al., 2010; D'Alpaos & Marani, 2016). This assumption arises from laboratory and field observations showing that vegetation reduces flow velocities and turbulent mixing, thereby enhancing deposition (Liu et al., 2024; Leonard & Croft, 2006; Nepf, 2012), and that vegetation can also trap suspended sediment directly on stems and leaves, albeit to a small degree (Li & Yang, 2009; Palmer et al., 2004; Mudd et al., 2010).

Duran Vinent et al. (2021) proposed a simple heuristic framework for predicting sediment deposition patterns on marsh platforms based on idealized fluid and sediment transport dynamics. Their model, which assumes quasi-steady tidal flows with no vegetation influence, predicts that the spatial distribution of sediment deposition is controlled primarily by tidal amplitude, marsh geometry, and grain settling rate, rather than by vegetation. Although this model provided potential insights into marsh evolution, it lacked a mechanistic justification for neglecting vegetation effects on flow and turbulent mixing, and resulting sediment deposition patterns.

Here we show, using analytical modeling and field data, that vegetation exerts little to no control on sediment deposition rates across tidal marsh basins, justifying that the simplifying assumptions of Duran Vinent et al. (2021) are, in fact, broadly valid for most tidal marsh conditions. We show that, in the context of tidal marshes, flow rates do not depend appreciably on vegetation for most of the marsh flood period, while turbulent mixing within canopies remains high enough to keep sediment well mixed throughout the water column. Consequently, sediment transport and deposition behave effectively as they would without vegetation. To first order, deposition rates are controlled by tidal properties, basin size, and grain settling rates—reflecting general dynamics of turbulent suspensions (Claudin et al., 2011; Duran Vinent et al., 2021).

2 Methods and Results

2.1 Flow velocity is independent of vegetation in marsh basins

Fluid flow and suspended sediment transport across tidal marsh platforms arise from the propagation of tidal water levels from channels into the basin interior. Because this process governs how sediment is distributed, understanding what sets characteristic flow velocities is central to predicting patterns of sediment deposition. Although dense vegetation is often assumed to slow tidal flow through drag, we find that, for typical marsh geometries and vegetation densities, flow velocities are set primarily by tidal water levels and basin geometry, not vegetation.

As a marsh platform floods from rising tides, the fluid transport rates $Q(x,t)$ tend to be highest near the channels ($x \sim 0$) and decrease towards the basin divide deep in the marsh ($x \sim L$) (Fig. 1). Flow rates across a marsh platform depend on water surface slopes, and could depend on vegetation characteristics generally (King et al., 2012;

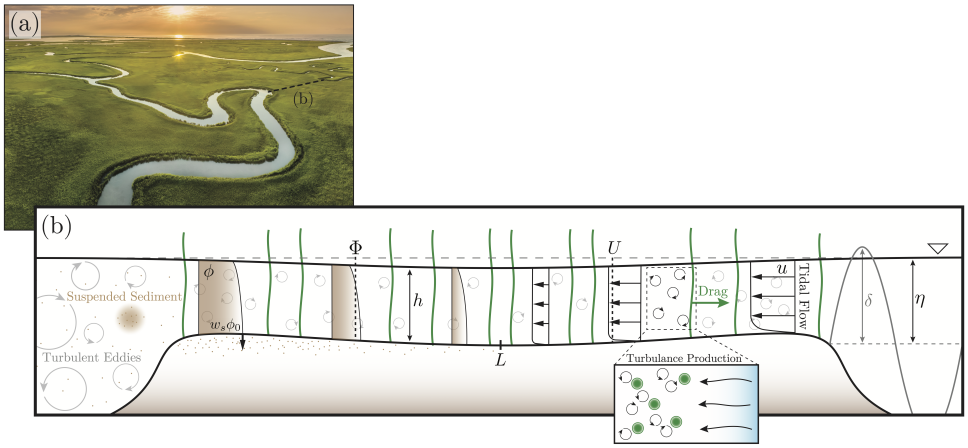

Figure 1. Overview of the tidal marsh system. (a) Aerial photo of a marsh with meandering channels separated by a vegetated marsh platform (photo by Ian Plant from Eastern Virginia, USA: ianplant.com). (b) An illustration of a cross section between two channels (e.g., in panel a). In the channels, suspended sediment is well mixed due to intense turbulence. As the marsh floods from rising tides, the suspended sediment concentration in the water column $\phi(z, x, t)$ is distributed across the platform—settling out of the water column at the bed at rate $w_s\phi_0(x, t)$. As the water flows over the platform, drag from the marsh vegetation (green) homogenizes the flow profile $u(z, x, t) \sim U(x, t)$. Simultaneously, small scale turbulence is produced in the wakes of vegetated stems (inset). This turbulence production keeps sediment suspended enough that the concentration profiles are nearly uniform $\phi(z, x, t) \sim \Phi(x, t)$. As the flow approaches the basin divide between channels, $x = L$, the flow and mixing rates as well as the concentration tend to vanish. However in a real marsh system the dynamics at the basin divide remain in flux and these quantities tend to remain residually present (e.g., Christiansen et al. (2000)).

Nepf, 2012). However, within marsh basins, for most of the flood period water surface slopes are small and the water surface over the entire marsh platform tends to rise and fall in step with the tide $\eta(x, t) \sim \eta_0(t)$—as reported in marsh observations (e.g., Christiansen et al. (2000)) and in detailed numerical simulations (e.g., Rinaldo et al. (1999)). As a consequence, the water flux must converge over the whole platform at that tidal rate, $\partial_t\eta_0 = -\partial_x Q$. Thus the flow rates are geometrically determined (Duran Vinent et al., 2021),

$$Q = hU \sim L\partial_t\eta_0(1 - x/L), \tag{1}$$

and thus are, to first order, determined by the tides $\partial_t \eta_0$ and the marsh basin size L—because larger marsh basins require more water input from channels. Therefore, to a good approximation marsh vegetation effects are not a controlling factor of the flow rate $u(z,x,t) \sim U(x,t) = Q(x,t)/h(x,t)$, where $h(x,t)$ is the local depth (Fig. 2b).

To test this simple geometric flow prediction (eq. 1) we examine the flow processes in more detail by directly modeling flow-vegetation interactions. In vegetated flows, fluid shear stresses driven by water-surface-slope-induced pressure gradients are opposed by drag forces on vegetation (Fig. 1) (Nepf, 2012). The characteristic fluid velocity u_V in vegetated flows scales as

$$\frac{u_V}{\sqrt{gD_V}} \sim \pm\sqrt{|\partial_x \eta|} \tag{2}$$

where g is gravity, $D_V \sim 1/a_V$ is a drag length that scales inversely with the frontal area of vegetation per unit volume a_V, and $\partial_x \eta$ is the water surface slope (Nepf, 2012; King et al., 2012) (see SI Section S1.1 for more details). On many marshes, vegetation is typically emergent for most, if not all, of the tidal flood period (e.g., Vandenbruwaene et al. (2015)), such that fluid shear stresses tend to vanish over nearly the entire flow depth (Nepf, 2012; King et al., 2012; Conde-Frias et al., 2023). This suggests that local flow profiles are well approximated by $u(z,x,t) \sim U(x,t) \sim u_V$ (Fig. 2a). In addition, for grain sizes which typically characterize marshes (often of order 10 μm; e.g., Christiansen et al. (2000)), the bed shear stress is usually not large enough to cause significant erosion within the marsh platform (see SI Section S1.5; Liu et al. (2024); Durán et al. (2011); Christiansen et al. (2000)). Here we focus on emergent vegetation, however, considering vegetation that becomes submerged for some portion of the flood period does not quantitatively change the results (see SI Section S1.4).

In Figure 2b,c we compare the geometric prediction for Q (eq. 1) to numerical solutions of the continuity equation $\partial_t \eta = -\partial_x (hU)$ for $U = u_V$ (eq. 2) and $h = \eta$ for simplicity—variations in bed elevation Z do not greatly alter these results (see SI Section S3). We impose boundary conditions $\eta(0,t) = \eta_0(t) = \delta \cos(2\pi t/T)$ and $\partial_x \eta(L,t) = 0$. Figure 2c shows that for high values of the velocity scale $\sqrt{gD_V}$ (eq. 2), compared to tidal velocity scale L/T (for tidal period T), the first order approximation for Q (eq. 1) holds for much of the flood period. As $\sqrt{gD_V}/(L/T)$ decreases the diffusion of tidal information from the channels becomes too slow for the water elevations over the platform to react to the changing tide—creating a lag between Q and $\partial_t \eta_0$. Typical values of frontal

vegetation areas are $1 \lesssim a_V \lesssim 10$ m^{-1} (Mudd et al., 2010; Nepf, 2012) and basin sizes $10 \lesssim L \lesssim 100$ m (e.g., SI Table S2; Duran Vinent et al. (2021)). Thus for sparse vegetated platforms and/or small basins $10^3 \lesssim \sqrt{gD_V}/(L/T) \lesssim 10^4$, and for dense platforms and/or large basin $10^2 < \sqrt{gD_V}/(L/T) \lesssim 10^3$, the first-order, geometric solution for Q in equation (1) is a good approximation for most of the marsh flood period (Fig. 2c).

Note that this result specific to tidal driven flows over marsh platform geometries, and necessarily applicable to other systems—for example deltas (Xu et al., 2022). We also note that vegetation is a dominant influence on channelizing flows and constructing complex channel networks in wetland systems in general (Van de Vijsel et al., 2023; Gourgue et al., 2024). We thus re-emphasize that these results are applicable to flow over a marsh platform and not at near or within channels.

Therefore, we have demonstrated that as suspended sediment is transported across the marsh (Fig. 1), the component of sediment deposition determined by the flow rate $u \sim U = Q/h$ can be considered approximately independent of vegetation effects. However, vegetation effects on turbulence may still contribute to changing the concentration of suspended sediment near the bed which would directly affect deposition rates. Because the near bed concentration is a reflection of turbulent mixing effects, a model of turbulent mixing in vegetated canopies must by analyzed.

2.2 Vegetation induced turbulent mixing

Although vegetation has little influence on the bulk flow velocities across a marsh, it does influence turbulent mixing rates. Within vegetated marsh platforms, shear-driven turbulence is suppressed, but small-scale turbulence is generated directly by flow-vegetation interactions—contributing to the vertical mixing of suspended sediments.

In the absence of vegetation, in tidal channels for example, high fluid shear stresses generate relatively large eddies that keep suspended sediment well mixed in the water column (see schematic in Fig. 1). In dense vegetated canopies on a marsh platform, the shear stress vanishes and therefore so does the self-production of turbulence from the velocity gradients (SI Section S1.2; Nepf (2012); King et al. (2012); Tanino and Nepf (2008)). However, the presence of vegetation leads to the direct generation of small-scale turbulence from flow-vegetation interactions (Tanino & Nepf, 2008) (Fig. 1). This turbulence

production gives rise to eddies with sizes on the order of the effective vegetation diameter d_V, and the turbulent kinetic energy k_V generated is balanced by viscous dissipation. This results in a characteristic eddy viscosity $\nu_t \sim d_V\sqrt{k_V}$ (King et al., 2012) defined by the characteristic turbulent kinetic energy (SI Section S1.2),

$$\frac{\sqrt{k_V}}{u_V} \sim (d_V/D_V)^{1/3} \sim \phi_V^{1/3}, \tag{3}$$

where $\phi_V \sim a_V d_V$ is the volume fraction of vegetation in the water column (Tanino & Nepf, 2008). On marsh platforms, vegetated frontal areas are between $1 \lesssim a_V \lesssim 10$ m^{-1} (Mudd et al., 2010; Nepf, 2012)—with typical values for *Spartina alterniflora* $a_V \sim 5$ m^{-1}. Stem densities vary between $10^2 \lesssim n_V \lesssim 10^3$ m^{-2} (Leonard & Luther, 1995; Leonard & Croft, 2006; Moskalski & Sommerfield, 2012; Tempest et al., 2015)—wtih typical values for *Spartina alterniflora* $n_V \sim 500$ m^{-2}. Thus effective plant 'diameters' vary around $d_V = a_V/n_V \sim \mathcal{O}(1)$ cm and volume fractions tend to be $0.01 \lesssim \phi_V \lesssim 0.1$ (Nepf, 2012).

In emergent or near emergent canopies on a marsh platform the eddy viscosity is given by the flow rate $u_V \sim U$ and a vegetation induced eddy length scale $\lambda/d_V \sim \phi_V^{1/3}$ such that

$$\nu_t \sim \lambda|U| \tag{4}$$

where U is given, to first order, by the geometric flux $Q = hU$ in equation (1). Thus vegetation directly produces turbulence within its canopy, which allows for the continued mixing of suspended sediment despite the lack of large-scale (shear-stress-produced) eddies. To evaluate how this vegetation-induced turbulence influences sediment deposition across marsh platform, we next model the evolution of suspended sediment concentrations over a full tidal cycle.

2.3 Sediment deposition patterns

Building on the flow and turbulence approximations above, we now examine how suspended sediment is transported and deposited across a marsh platform. Here we show that, under typical tidal and vegetation conditions, sediment concentrations remain nearly uniform throughout the water column for most of the tidal cycle due to vegetation induced mixing. Therefore, the resulting deposition patterns depend primarily on tidal geometry and grain settling rates, rather than vegetation characteristics.

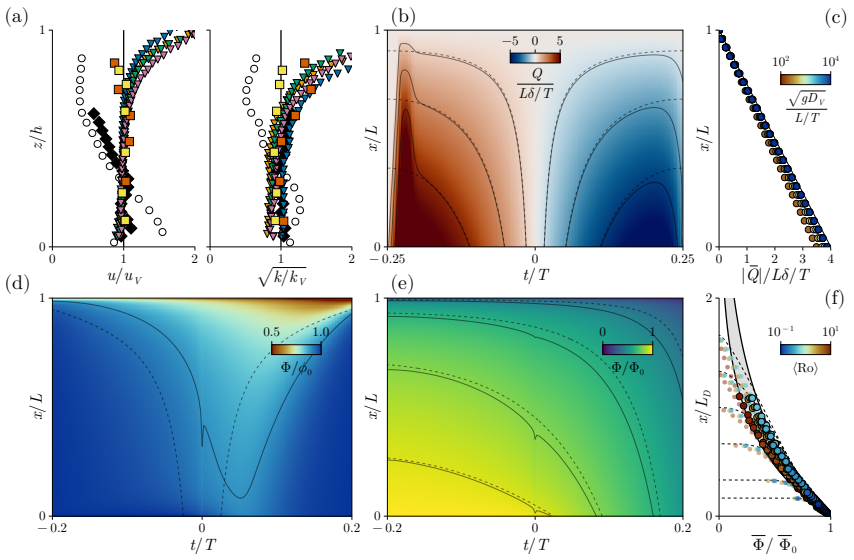

Figure 2. Fluid flow (a-c) and sediment transport (d-f) over a vegetated marsh platform. (a) Experimental profiles of flow speed $u(z)$ and turbulent kinetic energy $k(z)$, normalized by their characteristic vegetation influenced values u_V (eq. 2) and k_V (eq. 3), respectively (see SI Section S1). Elevations z/h are normalized by water depth h for emergent experiments or vegetation height for submerged experiments. Data shown from King et al. (2012) for submerged ($\bigtriangledown$) and emergent cylinders ($\square$). Real plants experiments with variable frontal areas $a_V(z)$: (King et al., 2012) ($\bigcirc$) and (Liu et al., 2024) ($\diamondsuit$). See SI Section S1.3 for more details on panel (a). (b) Numerical solutions of the flux $Q = hU$ from continuity for depth average velocities $U = u_V$ (eq. 2) with dashed contours from the geometric Q (eq. (1)). Here $\sqrt{gD_V}/(L/T) = 10^3$ with $L/\delta = 50$. (c) Time averaged flux magnitude $|\overline{Q}|$ for a range of vegetation densities and basin sizes (black line given by eq. (1)). (d) Ratio of the depth averaged suspended sediment concentration to the bed concentration $\Phi(x,t)/\phi_0(x,t)$ solved for the geometric approximated flow $U = Q/h$ (eq. 1, 5). Dashed line is Ro $= 1$—and also represents $\Phi/\phi_0 \sim 0.9$ from the approximation equation (8)—and solid line is the ratio $\Phi/\phi_0 \sim 0.9$ from the vertically resolved solution (eq. 5). (e) Map of average concentration relative to the constant channel concentration $\Phi(x,t)/\Phi_0$. Dashed lines are vegetation-independent solutions ($\phi_0 = \Phi$, eq. 6). For both (d) and (e), $w_s = \delta/T$ and $L/\delta = \delta/\lambda$. (f) Time averaged distributions $\overline{\Phi}(x)/\overline{\Phi}_0$ for a wide range of average Rouse numbers $\langle \text{Ro} \rangle$. Here distance x/L_D is rescaled by the decay length $L_D = \beta L(\delta/T)/w_s$ for $\beta = 3$. Filled markers are for $x/L \leq 2/3$ and smaller open markers for $x/L > 2/3$. Dashed lines are vegetation-independent solutions ($\phi_0 = \Phi$, eq. 6). Note that $\overline{\Phi} \to 0$ as $x \to L$. Grey shaded region are exponential curves for $\beta = 3$ and $\beta = 2$—most solution falls closer to $\beta = 3$, with the exception of large $\langle \text{Ro} \rangle$. Solutions to equation 5 are solved for flood times $t \in (-0.2, 0.2)$ (panel e) rather than $t \in (-0.25, 0.25)$ (panel b) to avoid numerical instabilities as $h \to 0$—this does not alter the results.

From the simplified geometric and quasi-steady approximations of the flow and turbulent mixing rates, we can greatly simplify the dynamics of sediment transport across a marsh platform. In general, the transport of the concentration of suspended sediment $\phi(z, x, t)$ can be modeled by mass conservation:

$$\partial_t \phi + u\partial_x \phi + w\partial_z \phi = w_s \partial_z \phi + \partial_z(\nu_s \partial_z \phi), \tag{5}$$

where w_s is the grain settling velocity and $\nu_s \simeq \nu_t$ is the sediment eddy viscosity—assuming negligible horizontal mixing for simplicity. The evolution of the depth averaged suspended sediment concentration $\Phi(x, t)$ is

$$h\partial_t \Phi + Q\partial_x \Phi = -w_s \phi_0, \tag{6}$$

where we have assumed vertically uniform flow $u(z, x, t) = U(x, t)$ (as in emergent vegetation). Here $w_s\phi_0(x, t)$ is the deposition rate, where $\phi_0(x, t) = \phi(0, x, t)$ is in general influenced by vegetation through the turbulent mixing rate $\nu_s \sim \nu_t$ (eq. 4). We thus see that if the turbulent mixing rate is large enough that $\phi_0 \sim \Phi$ and the flux Q is given by the geometric approximation (eq. 1) then the distribution of suspended sediment throughout the marsh platform $\phi(z, x, t) \sim \Phi(x, t)$ is *independent* of vegetation characteristics. And in this regime the tidal averaged concentration $\overline{\Phi}(x)$, and resulting deposition rate $w_s\overline{\Phi}(x)$, decays nearly exponentially away from marsh channels,

$$\overline{\Phi} \sim \overline{\Phi}_0 e^{-x/L_D}, \tag{7}$$

with $\overline{\Phi}_0 = \overline{\Phi}(0, t)$ (SI Section S2; Duran Vinent et al. (2021)). The deposition length scale L_D is dependent on the average flux scale relative to the settling rate $L_D \sim \langle Q \rangle / w_s \propto L\delta/Tw_s$ (Duran Vinent et al., 2021). This is the general behavior of turbulent suspensions at low Rouse numbers $\mathrm{Ro} = w_s h/\nu_s$ (Claudin et al., 2011).

A general approximation of the ratio $\Phi/\phi_0 = f(\mathrm{Ro})$ for high mixing rates relative to settling rates ($\mathrm{Ro} \lesssim 1$) is given (for depositional boundary conditions; see Si Section S2.1) by

$$\frac{\Phi}{\phi_0} \sim 1 - \frac{\mathrm{Ro}/6}{1 + \mathrm{Ro}/2}. \tag{8}$$

Thus for the high flow/mixing rates at the beginning and end of the period in which the marsh platform is flooded, the suspended sediment concentrations remain approximated homogeneous $\phi(z) \sim \Phi$ (eq. 1; Fig. 2b,d). Around high tide the flow and mixing rates cease and grains settle out of suspension. For tidal amplitude of order 1 m and grain settling rates of order 10^{-4} m/s, the timescale for grains settle out of suspension around

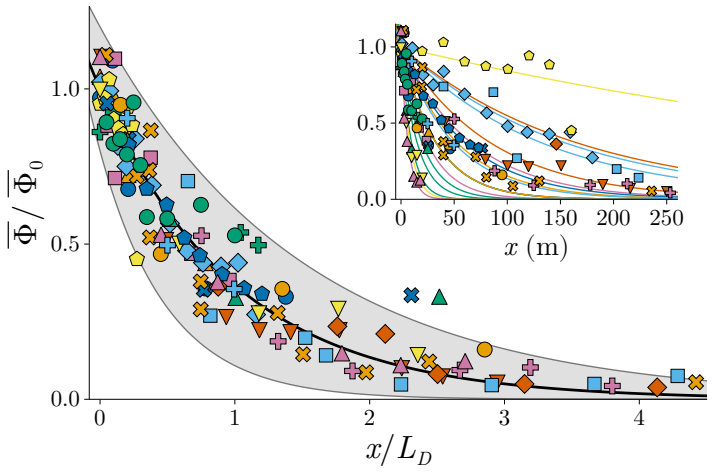

Figure 3. In-situ measurements of either suspended sediment concentrations or deposition rates for a wide variety of marshes around the world (colors and marker shapes show the different data sets). Distances from channels x are rescaled by the predicted decay length $L_D = 3L(\delta/T)/w_s$. The average channel concentration $\overline{\Phi}(0) = \overline{\Phi}_0$ (or deposition rate) is taken as a fit value. The black line is the predicted scaling $\overline{\Phi} = \overline{\Phi}_0 \exp(-x/L_D)$. The grey region varies L_D by ±50% and the channel concentration $\overline{\Phi}_0$ by ±20%. The inset plot shows non-rescaled distances x with the corresponded predicted exponential curves for a given marsh (i.e., a given L_D). Some data shown are obtained from Duran Vinent et al. (2021) Figure 3: Christiansen (1998); Coleman and Kirwan (2019); Coleman et al. (2020); French and Spencer (1993); van Proosdij et al. (2006). Other data used are: Butzeck et al. (2015); Reed et al. (1999); Wang et al. (1993); Temmerman et al. (2003); Leonard and Croft (2006); Stumpf (1983); Li and Yang (2009). For more information about the data and values of δ, T, w_s and L used see SI Table S2.

high tide is $h/w_s \sim \mathcal{O}(10^4)$ s. This is usually longer than the slack tidal period (around 1 h), and thus grains do not tend to have time to settle significantly before the flow/mixing rates increase again after slack tide (Fig. 2d).

To test the approximation that sediment concentrations and deposition rates are independent of vegetation, we numerically integrate sediment continuity equation (5) for the full vertical sediment concentration profiles over a tidal cycle $\phi(z, x, t)$, using the first order geometric approximation for the flow rate $U(x, t) = (L - x)\partial_t \eta_0/h$ (eq. 1) and eddy viscosity $\nu_s(x, t) = \lambda|U|$ (eq. 4). Figure 2d,e shows example solutions for a typical average Rouse number $\langle \mathrm{Ro} \rangle = w_s\langle h \rangle/\lambda\langle U \rangle$, where $\langle h \rangle = 2\delta/\pi$ and $\langle U \rangle = \langle Q \rangle/\langle h \rangle$

with $\langle Q \rangle = 2\delta L/T$. We find that for a typical range of Rouse numbers $0.1 \lesssim \langle \mathrm{Ro} \rangle \lesssim 10$ the vertical distribution of suspended sediment is relatively homogeneous such that $\phi_0(x,t) \sim \Phi(x,t)$ for much of the platform area and flood period, and thus the concentration does not on average depend much on vegetation characteristics (Fig. 2f). We note that concentrations in this model vanish with the flow at the basin divide $x \sim L$. However, in real marshes residual flow and mixing is present in the central basin and the suspended sediment concentration does not actually vanish $\phi(z, L, t) \gtrsim 0$ (e.g., Christiansen et al. (2000)) and thus we don't expect this model to be quantitatively accurate near the basin divide $x \sim L$ (Duran Vinent et al., 2021). When comparing the time averaged concentrations $\overline{\Phi}(x)$ to idealized predictions (taking $\phi_0 = \Phi$ in eq. 6) we find that over a wide range of $\langle \mathrm{Ro} \rangle$ the exponential decay approximation (eq. 7) works well (for $x \lesssim L$). The exponential decay length scales as $L_D/L \sim \beta(\delta/T)/w_s$ (Duran Vinent et al., 2021), with $\beta \sim 3$ for most $\langle \mathrm{Ro} \rangle$ and $\beta \sim 2$ for exceedingly high $\langle \mathrm{Ro} \rangle \gtrsim 10$. In Supporting Information Section S3 we test that this deposition scaling is robust for variations in bed elevation (i.e., flood frequency) and bed slope. For upland marshes—marsh platforms bordered by a channel on one side and sloping upward to subaerial land on the other—we find similar behavior, however the effective basin size L is roughly half the maximum flood length (which is determined by the upland slope and tidal range; see SI Figure S4).

In summary, the simplified quasi-steady, geometric tidal flows over a vegetated marsh platform (eq. 1-4) suggest that the turbulence induced by vegetation is large enough to maintain sediment suspension throughout the tidal cycle (Fig. 2d-f). This renders the sediment concentration profiles nearly homogeneous and thus independent of the vegetation within the flow (eq. 6), suggesting that the tidal-averaged distribution of suspended sediment concentration $\overline{\Phi}(x)$ and sediment deposition $\sim w_s\overline{\Phi}(x)$ across a platform follows a simple decay law (eq. 7) that depends only on basin size L, grain settling rates w_s, and tidal properties δ, T.

While this represents a simplified approximation of the inherently variable tidal and sediment transport dynamics, the prediction that suspended sediment concentrations and deposition rates are largely independent of vegetation is consistent with global observations across marshes spanning a wide range of vegetation types and densities (Fig. 3). Thus despite considering 2D flow, emergent vegetation, ignoring grain size distributions and flocculation, etc., the model prediction agreement with the wide range of observa-

tions in Figure 3 supports the robustness of this simplified framework for understanding intertidal marsh flow and sediment transport dynamics, and resulting long-term marsh evolution.

3 Discussion and Conclusions

We have demonstrated that the depositional dynamics of suspended sediments across a marsh with dense vegetation are largely independent of the vegetation characteristics themselves. Rather, sediment deposition rates are controlled primarily by tidal properties, marsh platform size, and grain settling rates. Vegetation still plays a critical stabilizing role by preventing erosion of the marsh platform, but it does not, to first order, control the bulk flow rates or sediment deposition patterns. These results challenge assumptions that vegetation controls platform-wide deposition, but they remain consistent with evidence that vegetation primarily influences sediment routing near marsh–channel edges rather than in interior platforms (Gourgue et al., 2024).

Our finding suggests that inorganic and organic components of marsh accretion are effectively decoupled, meaning that the rate of sediment deposition can be predicted without explicitly resolving vegetation density or canopy structure. This greatly simplifies models of marsh evolution, allowing the tidal-averaged deposition rate across a platform (eq. 7) to be represented with a reduced-order, mechanistic framework. Such simplifications are particularly valuable for regional- to global-scale modeling of marsh resilience to sea-level rise. Additionally, by identifying the primary pattern (eq. 7) and controls that set sediment depositional scaling—tidal properties, basin size, and grain settling rates (Duran Vinent et al., 2021)—uncertainties in predicting critical rates of sea level rise (beyond which marshes drown) are then reduced to the uncertainties in empirical observations of organic accretion rates on a given marsh.

Although this analysis focuses mainly on vegetation that remains emergent throughout the tidal period, we expect similar results for submerged vegetation. Submergence tends to enhance tidal communication across the basin and increase mixing from shear-generated turbulence, reinforcing the same first-order behavior described here (SI Section S1.4, S2.1). The resulting near-homogeneous sediment distributions (SI Section S2) are thus effectively independent of vegetation, consistent with the generalized turbulent suspension dynamics of low Rouse number flows (Claudin et al., 2011). The scale col-

lapse in Figure 3—spanning marshes with a wide range of vegetation types and densities, including partially submerged canopies—further supports this conclusion.

In summary, this work provides a mechanistic justification for relatively simple models of marsh evolution and formally isolates the main controls of sediment deposition across tidal marshes. The dominant role of vegetation lies in providing organic accretion and stabilizing deposited sediments, but is not a controlling factor in determining mineral sediment accretion rates. This distinction shifts the predictive uncertainty in marsh evolution from resolving canopy-scale flows over subtidal timescales to constraining sediment supply and vegetation deposition rate dynamics.

Open Research Section

Code used to generate numerical results in Figure 2d-f and Figures S1, S3, S4 will be made available on GitHub (repository to generated after paper is accepted). Vegetated flow experiments used in Figure 2a are obtained from King et al. (2012) and Liu et al. (2024). Sediment concentration/deposition data used in Figure 3 were obtained from a range of publications listed in Table S2.

Conflict of Interest declaration

The authors declare there are no conflicts of interest for this manuscript.

Acknowledgments

This work was supported by the National Science Foundation Geomorphology and Land Use Program, grant number 2016068.

References

Butzeck, C., Eschenbach, A., Gröngröft, A., Hansen, K., Nolte, S., & Jensen, K. (2015). Sediment deposition and accretion rates in tidal marshes are highly variable along estuarine salinity and flooding gradients. *Estuaries and Coasts*, *38*, 434–450.

Campbell, A. D., Fatoyinbo, L., Goldberg, L., & Lagomasino, D. (2022). Global hotspots of salt marsh change and carbon emissions. *Nature*, *612*(7941), 701–706.

Christiansen, T. (1998). *Sediment deposition on a tidal salt marsh.* University of Virginia.

Christiansen, T., Wiberg, P. L., & Milligan, T. (2000). Flow and sediment transport on a tidal salt marsh surface. *Estuarine, Coastal and Shelf Science*, *50*(3), 315–331.

Claudin, P., Charru, F., & Andreotti, B. (2011). Transport relaxation time and length scales in turbulent suspensions. *Journal of Fluid Mechanics*, *671*, 491–506.

Coleman, D. J., Ganju, N. K., & Kirwan, M. L. (2020). Sediment delivery to a tidal marsh platform is minimized by source decoupling and flux convergence. *Journal of Geophysical Research: Earth Surface*, *125*(8), e2020JF005558.

Coleman, D. J., & Kirwan, M. L. (2019). The effect of a small vegetation dieback event on salt marsh sediment transport. *Earth Surface Processes and Landforms*, *44*(4), 944–952.

Conde-Frias, M., Ghisalberti, M., Lowe, R., Abdolahpour, M., & Etminan, V. (2023). The near-bed flow structure and bed shear stresses within emergent vegetation. *Water Resources Research*, *59*(4), e2022WR032499.

Durán, O., Claudin, P., & Andreotti, B. (2011). On aeolian transport: Grain-scale interactions, dynamical mechanisms and scaling laws. *Aeolian Research*, *3*(3), 243–270.

Duran Vinent, O., Herbert, E. R., Coleman, D. J., Himmelstein, J. D., & Kirwan, M. L. (2021). Onset of runaway fragmentation of salt marshes. *One Earth*, *4*(4), 506–516.

D'Alpaos, A., & Marani, M. (2016). Reading the signatures of biologic–geomorphic feedbacks in salt-marsh landscapes. *Advances in water resources*, *93*, 265–275.

Fagherazzi, S., Mariotti, G., Leonardi, N., Canestrelli, A., Nardin, W., & Kearney, W. S. (2020). Salt marsh dynamics in a period of accelerated sea level rise. *Journal of Geophysical Research: Earth Surface*, *125*(8), e2019JF005200.

French, J. R., & Spencer, T. (1993). Dynamics of sedimentation in a tide-dominated backbarrier salt marsh, norfolk, uk. *Marine Geology*, *110*(3-4), 315–331.

Gourgue, O., Belliard, J.-P., Xu, Y., Kleinhans, M. G., Fagherazzi, S., & Temmerman, S. (2024). Dense vegetation hinders sediment transport toward saltmarsh interiors. *Limnology and Oceanography Letters*, *9*(6), 764–775.

King, A., Tinoco, R., & Cowen, E. (2012). A k–ε turbulence model based on the scales of vertical shear and stem wakes valid for emergent and submerged vegetated flows. *Journal of Fluid Mechanics*, *701*, 1–39.

Kirwan, M. L., Guntenspergen, G. R., d'Alpaos, A., Morris, J. T., Mudd, S. M., & Temmerman, S. (2010). Limits on the adaptability of coastal marshes to rising sea level. *Geophysical research letters*, *37*(23).

Kirwan, M. L., & Megonigal, J. P. (2013). Tidal wetland stability in the face of human impacts and sea-level rise. *Nature*, *504*(7478), 53–60.

Kirwan, M. L., & Murray, A. B. (2007). A coupled geomorphic and ecological model of tidal marsh evolution. *Proceedings of the National Academy of Sciences*, *104*(15), 6118–6122.

Leonard, L. A., & Croft, A. L. (2006). The effect of standing biomass on flow velocity and turbulence in spartina alterniflora canopies. *Estuarine, Coastal and Shelf Science*, *69*(3-4), 325–336.

Leonard, L. A., & Luther, M. E. (1995). Flow hydrodynamics in tidal marsh canopies. *Limnology and oceanography*, *40*(8), 1474–1484.

Li, H., & Yang, S. (2009). Trapping effect of tidal marsh vegetation on suspended sediment, yangtze delta. *Journal of coastal research*, *25*(4), 915–924.

Liu, C., Shan, Y., He, L., Li, F., Liu, X., & Nepf, H. (2024). Plant morphology impacts bedload sediment transport. *Geophysical Research Letters*, *51*(12), e2024GL108800.

Marani, M., Da Lio, C., & D'Alpaos, A. (2013). Vegetation engineers marsh morphology through multiple competing stable states. *Proceedings of the National Academy of Sciences*, *110*(9), 3259–3263.

Marani, M., D'Alpaos, A., Lanzoni, S., Carniello, L., & Rinaldo, A. (2007). Biologically-controlled multiple equilibria of tidal landforms and the fate of the venice lagoon. *Geophysical Research Letters*, *34*(11).

Marani, M., D'Alpaos, A., Lanzoni, S., Carniello, L., & Rinaldo, A. (2010). The importance of being coupled: Stable states and catastrophic shifts in tidal biomorphodynamics. *Journal of Geophysical Research: Earth Surface*, *115*(F4).

Morris, J. T., Sundareshwar, P., Nietch, C. T., Kjerfve, B., & Cahoon, D. R. (2002). Responses of coastal wetlands to rising sea level. *Ecology*, *83*(10), 2869–2877.

Moskalski, S. M., & Sommerfield, C. K. (2012). Suspended sediment deposition and trapping efficiency in a delaware salt marsh. *Geomorphology*, *139*, 195–204.

Mudd, S. M., D'Alpaos, A., & Morris, J. T. (2010). How does vegetation affect sedimentation on tidal marshes? investigating particle capture and hydrodynamic controls on biologically mediated sedimentation. *Journal of Geophysical Research: Earth Surface*, *115*(F3).

Nepf, H. M. (2012). Flow and transport in regions with aquatic vegetation. *Annual review of fluid mechanics*, *44*(1), 123–142.

Palmer, M. R., Nepf, H. M., Pettersson, T. J., & Ackerman, J. D. (2004). Observations of particle capture on a cylindrical collector: Implications for particle accumulation and removal in aquatic systems. *Limnology and Oceanography*, *49*(1), 76–85.

Reed, D. J., Spencer, T., Murray, A. L., French, J. R., & Leonard, L. (1999). Marsh surface sediment deposition and the role of tidal creeks: implications for created and managed coastal marshes. *Journal of Coastal conservation*, *5*, 81–90.

Rinaldo, A., Fagherazzi, S., Lanzoni, S., Marani, M., & Dietrich, W. E. (1999). Tidal networks: 2. watershed delineation and comparative network morphology. *Water Resources Research*, *35*(12), 3905–3917.

Stumpf, R. P. (1983). The process of sedimentation on the surface of a salt marsh. *Estuarine, Coastal and Shelf Science*, *17*(5), 495–508.

Tanino, Y., & Nepf, H. M. (2008). Lateral dispersion in random cylinder arrays at high reynolds number. *Journal of Fluid Mechanics*, *600*, 339–371.

Temmerman, S., Bouma, T. J., Van de Koppel, J., Van der Wal, D., De Vries, M. B., & Herman, P. M. (2007). Vegetation causes channel erosion in a tidal landscape. *Geology*, *35*(7), 631–634.

Temmerman, S., Govers, G., Wartel, S., & Meire, P. (2003). Spatial and temporal factors controlling short-term sedimentation in a salt and freshwater tidal marsh, scheldt estuary, belgium, sw netherlands. *Earth Surface Processes and Landforms: The Journal of the British Geomorphological Research Group*, *28*(7), 739–755.

Tempest, J. A., Möller, I., & Spencer, T. (2015). A review of plant-flow interactions on salt marshes: The importance of vegetation structure and plant mechanical characteristics. *Wiley Interdisciplinary Reviews: Water*, *2*(6), 669–681.

Vandenbruwaene, W., Schwarz, C., Bouma, T., Meire, P., & Temmerman, S. (2015). Landscape-scale flow patterns over a vegetated tidal marsh and an unvegetated tidal flat: Implications for the landform properties of the intertidal floodplain. *Geomorphology*, *231*, 40–52.

Van de Vijsel, R. C., van Belzen, J., Bouma, T. J., van der Wal, D., Borsje, B. W., Temmerman, S., ... van de Koppel, J. (2023). Vegetation controls on channel network complexity in coastal wetlands. *Nature communications*, *14*(1), 7158.

van Proosdij, D., Davidson-Arnott, R. G., & Ollerhead, J. (2006). Controls on spatial patterns of sediment deposition across a macro-tidal salt marsh surface over single tidal cycles. *Estuarine, Coastal and Shelf Science*, *69*(1-2), 64–86.

Wang, F. C., Lu, T., & Sikora, W. B. (1993). Intertidal marsh suspended sediment transport processes, terrebonne bay, louisiana, usa. *Journal of Coastal Research*, 209–220.

Xu, Y., Esposito, C. R., Beltrán-Burgos, M., & Nepf, H. M. (2022). Competing effects of vegetation density on sedimentation in deltaic marshes. *Nature communications*, *13*(1), 4641.

Zhang, Y., Rowland, J. C., Xu, C., Wolfram, P. J., Svyatsky, D., Moulton, J. D., ... Pasqualini, D. (2020). Understanding the eco-geomorphologic feedback of coastal marsh under sea level rise: Vegetation dynamic representations, processes interaction, and parametric sensitivity. *Journal of Geophysical Research: Earth Surface*, *125*(11), e2020JF005729.

Supporting Information for "Vegetation Does Not Control Suspended Sediment Deposition in Salt Marshes"

C. W. Lester[1,2], A. B. Murray[1], and Orencio Durán Vinent[3], Marco Marani[4],

Andrea D'Alpaos[5], Sonia Silvestri[6], Tegan Blount[5], Zhicheng Yang[1]

[1]Division of Earth and Climate Sciences, Duke University, Durham, NC, USA

[2]Department of Physics and Physical Oceanography, University of North Carolina Wilmington, Wilmington, NC, USA

[3]Department of Ocean Engineering, Texas A&M University, College Station, TX, USA

[4]Department of Civil, Environmental, and Architectural Engineering, University of Padova, Padova, Italy

[5]Department of Geosciences, University of Padova, Padova, Italy

[6]Department of Biological, Geological and Environmental Sciences, University of Bologna, Padova, Italy

Contents of this file

1. Sections S1 to S3

2. Figures S1 to S4

3. Tables S1 to S2

Corresponding author: C. W. Lester, Division of Earth and Climate Sciences, Duke University, Durham, NC, USA; Department of Physics and Physical Oceanography, University of North Carolina Wilmington, Wilmington, NC, USA (connerlester@duke.edu, lesterc@uncw.edu)

Introduction The contents in this Supporting Information (SI) file expand on the analytical modeling and results. Here we provide detailed derivations and extra information not elaborated on in the main text—i.e., important details for model and result robustness. We also provide section S1.3 and table S1 expanding on the data shown in main text figures 2 and 3, respectively. The SI table is a reference for all symbols used, their definitions, and scales.

S1. Fluid Dynamics Through Vegetation

The fluid flow over a marsh platform is assumed to be in quasi-steady state—i.e., the flow relaxes quickly in space and time to equilibrium. This approximation is valid for much of the flood period but not strictly valid during the very initial stages of flooding (e.g., as the bore wave propagates towards the basin divide; see Section 1.1.1).

S1.1. Flow Velocity

Given the quasi-steady flow approximation, the gradients in momentum flux (shear stress) τ_u are balanced by gravitational pressure gradients and vegetation drag:

$$\rho^{-1}\partial_z\tau_u \sim -g\partial_x\eta + \frac{1}{2}C_D\frac{a_V}{1-\phi_V}|\boldsymbol{u}|u$$

with drag coefficient C_D, frontal vegetation area per unit volume a_V and the volume fraction of vegetation ϕ_V.

Following Tanino and Nepf (2008a), the drag coefficient can be broken down into viscous and turbulent/pressure components,

$$C_D \sim 2\frac{\mathrm{Re}_V^T}{ud_V/\nu} + C_\infty, \tag{S1}$$

where ud_V/ν is the vegetation Reynolds number based on the effective stem diameter d_V, $\mathrm{Re}_V^T \gtrsim \mathcal{O}(10)$ is a transitional Reynolds number for an array of vegetation and $C_\infty \gtrsim 1$ is the turbulent/pressure drag coefficient. (Tanino and Nepf (2008a) found $\mathrm{Re}_V^T \sim 30$ and $C_\infty \sim 1 + 8\phi_V$ for an array of rigid cylinders.) With this the balance of forces $\partial_z \tau_u = 0$ gives rise to the characteristic vegetation velocity

$$\frac{u_V}{U_V} = \mathcal{R}^{-1}\left(\sqrt{1+\mathcal{R}^2} - 1\right) \tag{S2}$$

where $\mathcal{R} = C_\infty \mathrm{Re}_V/\mathrm{Re}_V^T$ is a Reynolds number ratio based on the vegetation Reynolds number $\mathrm{Re}_V = U_V d_V/\nu$ defined by the characteristic turbulent velocity scale

$$\frac{U_V}{\sqrt{gD_V}} = \pm\sqrt{|\partial_x \eta|} \tag{S3}$$

where the vegetation drag length is given by $D_V^{-1} = \frac{1}{2}C_\infty \frac{a_V}{1-\phi_V}$. If we take the flow depth to be much greater than the viscous sublayer thickness (which is an assumption that $h/d_V \gg 1$; see Section S1.5; Etminan, Ghisalberti, and Lowe (2018); Conde-Frias, Ghisalberti, Lowe, Abdolahpour, and Etminan (2023); Yang, Kerger, and Nepf (2015)) then the steady depth averaged velocity in emergent vegetation is well approximated by $U \equiv \frac{1}{h}\int_0^h u\mathrm{d}z \simeq u_V$. Additionally, given that natural marsh systems are generally turbulent with $\mathcal{R} \gg 1$ (at least outside of the viscous sublayer), the flow velocity throughout most of the water depth tends towards $u_V \sim U_V$. In the main text equation (2) we assume $\mathcal{R} \gg 1$ and present $u_V = U_V$ for brevity.

As in the main text, we use $U \sim U_V$ (eq. S3) to solve for the flow over a tidal cycle across a marsh platform using mass conservation $\partial_t h = -\partial_x(hU)$ and compare the vegetated solution to the geometric, quasi-steady approximation that $h(x,t) \sim h(0,t)$ and

thus $Q_0(x,t) \sim (L-x)\partial_t h(0,t)$. Figure S1 compares solutions for a range of parameters representing densely vegetated marshes, showing that for most of the flood period the geometric approximation $Q \sim Q_0$ works well.

S1.1.1. Initial Bore Propagation

At the very initial flood stage, $t \gtrsim t_0$, a bore wave propagates from the channel edge $x = 0$ towards the basin divide $x \to L$. This is a transient period where the flow is highly advective and not quasi-steady as assumed here. Once the bore reaches the basin divide the transience quickly relaxes and only then does the quasi-steady flow approximation hold (for almost of the rest of the tidal period until the very last moments of flooding; see Figure S1.) This bore wave should in principle propagate across the marsh platform at speed $c_B \sim \sqrt{gh_0} \sim \sqrt{g\partial_t\eta_0\Delta t}$, where $h_0(t = t_0 + \Delta t) \sim \partial_t\eta_0\Delta t$ is the initial water surface height at the marsh edge. (Here we are ignoring vegetation effects on c_B as a first approximation.) In the quasi-steady framework (eq. S3) the bore wave propagates across the platform at a constant rate $c_{B_V} = (gD_V\partial_t\eta_0)^{1/3}$. The time it takes the quasi-steady bore wave to reach the basin divide $\Delta t_{B_V} = L/(gD_V\partial_t\eta_0)^{1/3}$ where the transient bore time is $\Delta t_B \sim L^{2/3}/(g\partial_t\eta_0)^{1/3}$. Thus the quasi-steady approximation is conservative in the sense that the true bore wave likely reaches the basin divide quicker than assumed here:

$$\frac{\Delta t_B}{\Delta t_{B_V}} \sim \left(\frac{D_V}{L}\right)^{1/3} < 1.$$

As shown in Figure S1, once the bore wave reaches the basin divide the flux can be well described by the geometric approximation $Q \sim Q_0$. Given simulations using the quasi-steady approximation of the flow velocity (eq. S3) likely produce slower bore wave

propagation than reality, we expect even better agreement that $Q \sim Q_0$ when considering the more realistic transient bore propagation.

S1.2. Turbulent Kinetic Energy

The effects of turbulence on suspended sediment transport is encapsulated in the turbulent/eddy viscosity $\nu_t \simeq \nu_s$. The simplest (0-th order) eddy viscosity model assumes turbulence is generated directly from gradients in the flow $\nu_t \sim \ell^2|\partial_z u|$, where $\ell(z)$ is the characteristic eddy size or mixing length. This simplified approach works well for unobstructed flows (no vegetation). However, in vegetated flow this model predicts that the eddy viscosity would vanish as the fluid shear stress vanishes—and turbulent mixing of suspended sediment would cease, possibly increasing deposition rates as grains settle out of suspension. A higher order approach models the eddy viscosity by conserving turbulent kinetic energy k as $\nu_t \propto \ell\sqrt{k}$ (King et al., 2012). As with conserving momentum in quasi-steady state, the gradients in turbulent kinetic energy flux τ_k are balanced by the production and dissipation of turbulent kinetic energy:

$$\partial_z \tau_k \sim \nu_t(\partial_z u)^2 + \frac{1}{2} C_D \frac{a_V}{1-\phi_V}|u|^3 - \varepsilon.$$

Here the production of turbulence arises from velocity gradients as well as from vegetation itself. When the turbulent kinetic energy flux is balanced in unobstructed flows (no vegetation), the viscous dissipation rate $\varepsilon \propto k^{3/2}/\ell$ is balanced by the turbulence production from velocity gradients and the 0-th order eddy viscosity model is recovered. In dense vegetation the flux of turbulent kinetic energy vanishes with the shear stress and kinetic energy production from vegetation is balanced by viscous dissipation. It is taken that

this balance can be described by turbulent/pressure induced eddy production such that $\varepsilon \propto D_V^{-1} u_V^3$ (Tanino & Nepf, 2008b). This gives a characteristic turbulent kinetic energy in vegetated canopies

$$\frac{\sqrt{k_V}}{u_V} = \gamma \left(\ell_V / D_V\right)^{1/3} \tag{S4}$$

where $\gamma \sim \mathcal{O}(1)$ is a proportionality constant. The production of eddies comes from vortex shedding and the characteristic mixing length scale is set by the effective diameter $\ell_V \sim d_V$ (Tanino & Nepf, 2008b)—or ℓ_V is set by the spacing between plants when this spacing is smaller than d_V, which occurs when $\phi_V \gtrsim 0.75$ (an unrealistic value to find on marshes). The eddy viscosity in vegetated canopies $\nu_t \sim \ell_V \sqrt{k_V}$ is approximated by

$$\nu_t \sim \phi_V^{1/3} \ell_V u_V \sim \lambda u_V$$

where $\lambda \sim \ell_V (\ell_V / D_V)^{1/3} \sim d_V \phi_V^{1/3}$ using $D_V \sim 1/a_V$ and $\ell_V \sim d_V$. For $u_V \sim U_V \sim U$ we recover Equation (4) in the main text.

S1.3. Vegetated Flow Experiments

In Figure 2a we present data from experiments of flow through cylinders and real plants. The characteristic velocity used in the rescaling of the data takes into account the viscous correction from $\mathcal{R}$ in equation (S2).

All parameter values needed for u_V and k_V were provided in King et al. (2012), including $\partial_x \eta$ and Re_V^T. For all King et al. (2012) profiles of k_V we take $\gamma = 0.87$. Experiments used in Figure 2a from King et al. (2012): submerged cylinder experiments S1-S4 ($\bigtriangledown$), cylinder heights $h_V/h \sim 3/4$; emergent cylinders experiments E1-E2 ($\square$); live plant experiment

(◯), plant height $h_V = h$ with vertically variable plant area $a_V(z)$ was taken to be its depth averaged value for approximating u_V and k_V.

For emergent live *Typha latifolia* experiments of Liu et al. (2024) (◇), drag coefficients were not provided so we take $C_D = 1$ and $u_V = U_V$. And we assume the surface slope matched the bed slope $|\partial_x \eta| = 0.005$. And we used $\gamma = 1.1$. As above the vertically variable plant area $a_V(z)$ was taken to be its depth averaged value for approximating u_V and k_V.

S1.4. Submerged Vegetation

A conservative model of submerged vegetation separates flow into the canopy layer ($z < h_V$) where vegetation drag forces balances pressure gradients and the free-stream layer ($h_V < z < h$) where the gradients in shear stress are balanced by the pressure gradient. This gives a shear stress profile $\tau_u \sim 0$ in the canopy layer and $\tau_u \sim \rho u_*^2(1 - z/h)$ in the free-stream layer, where $u_*^2 = gh|\partial_x \eta|$. In the free-stream layer the eddy mixing length takes the form $\ell \sim \kappa(z + z_0 - h_V)\sqrt{1 - z/h}$ where the 'roughness' $z_0 = \ell_V/\kappa\sqrt{1 - h_V/h}$, given by the canopy mixing length $\ell_V \sim d_V$ and the Von Karman constant $\kappa \simeq 0.4$, ensures $\ell(h_V) = \ell_V$. This model gives the piecewise flow velocity profile $u \sim u_V$ (eq. S2) for $z < h_V$ and

$$u \sim u_V + \frac{u_*}{\kappa} \log\left(\frac{z + z_0 - h_V}{z_0}\right) \quad \text{for} \quad h_V < z < h. \tag{S5}$$

The depth averaged flow velocity $U = \frac{1}{h}\int_0^h u \mathrm{d}z$ for fully turbulent flow ($u_V \sim U_V$) is

$$\frac{U}{U_V} \sim 1 + \frac{1}{\kappa}\sqrt{\frac{h}{D_V}}\left[\left(1 + \frac{z_0}{h} - \frac{h_V}{h}\right)\log\left(\frac{1 + z_0/h - h_V/h}{z_0/h}\right) + \frac{h_V}{h} - 1\right] \quad \text{for} \quad h > h_V. \tag{S6}$$

In Figure S1 we compare the effects of submerged vegetation on the flow. For $h_V = \delta/2$, once the vegetation becomes submerged $h(x,t) > h_V$ the water surface elevations quickly relax to $h(x,t) \sim h(0,t)$ and the flux quickly relaxes to the geometric approximation $Q(x,t) \sim Q_0(x,t) = (L-x)\partial_t h(0,t)$.

The turbulent kinetic energy in the free-stream layer is given by the balance $k \propto \tau$ or $\sqrt{k} \sim u_* \sqrt{1 - z/h}$. Thus the eddy viscosity takes the piecewise form $\nu_t = \nu_{tV} \sim (\ell_V/D_V)^{1/3} U_V \ell_V$ for $z < h_V$ and

$$\nu_t \sim \kappa u_* (z + z_0 - h_V)\left(1 - \frac{z}{h}\right) \quad \text{for} \quad h_V < z < h. \tag{S7}$$

The depth-averaged eddy viscosity $N_t = \frac{1}{h}\int_0^h \nu_t \mathrm{d}z$ is given by

$$\frac{N_t}{\nu_{tV}} \sim \frac{h_V}{h} + \kappa \frac{u_* h}{\nu_{tV}} \left[\left(\frac{1}{6} + \frac{h_V}{h} - \frac{z_0}{h} \right) \left(1 - \frac{h_V^2}{h^2} \right) - \left(\frac{h_V}{h} - \frac{z_0}{h} \right) \left(1 - \frac{h_V}{h} \right) \right] \quad \text{for} \quad h > h_V. \tag{S8}$$

The ratio $N_t/\nu_{tV} \gg 1$ for well-submerged canopies ($h > h_V$) as the free-stream component of the average eddy viscosity increases rapidly as $N_t \sim h^{3/2}$. For example, for $h_V/\delta = 1/2$, $N_t/\nu_{tV} \sim 10$ for $h/h_V \sim 3/2$ ($h/\delta \sim 3/4$) and $N_t/\nu_{tV} \sim 20$ for $h/h_V \sim 2$ ($h/\delta \sim 1$). This suggests that once vegetation becomes submerged $h(x,t) > h_V$ the turbulent mixing of suspended sediment becomes greatly enhanced—allowing suspended sediment concentration profiles to become more homogeneous $\phi(z) \sim \Phi$.

S1.5. Bed Shear Stress

The bed shear stress $\tau_b = \tau_u(z = 0)$ is a critical quantity because if τ_b exceeds a threshold value τ_{th} the sediment surface begins to eroded. In the approximation that the near-bed

shear stresses are dominated by viscous effects we can take

$$\rho^{-1}\partial_z\tau_u \sim \nu\partial_{zz}u \sim -g\partial_x\eta + \mathrm{Re}_V^T \frac{a_V}{1-\phi_V}\frac{\nu}{d_V}u$$

where we have used $C_D \sim 2\mathrm{Re}_V^T/(ud_V/\nu)$ near the bed. From this we can derive a rough approximation of the near bed flow velocity

$$\lim_{z/\delta_\nu \to 0} \frac{u(z)}{u_V} \sim \sigma\left(1 - e^{-z/\delta_\nu}\right), \tag{S9}$$

where δ_ν is a length scale that sets the viscous sublayer thickness. The factor $\sigma(\mathcal{R})$ is a viscous drag relaxation scale based on the Reynolds number ratio $\mathcal{R}$ defined by $\sigma = \frac{1}{2}\mathcal{R}^2/(\sqrt{1+\mathcal{R}^2}-1)$, which is $\sigma \sim 1$ for $\mathcal{R} \lesssim 1$. However because $\mathcal{R} \gg 1$, nonlinear drag effects are important outside of the viscous sublayer δ_ν, thus this profile $u(z)$ is only accurate for $z \lesssim \delta_\nu$. The viscous sublayer thickness scale is defined by $\delta_\nu = \sqrt{\frac{1-\phi_V}{\mathrm{Re}_V^T n_V}}$ which can be rewritten using $\phi_V \propto a_V d_V = n_V d_V^2$ as $\delta_\nu/d_V \propto \phi_V^{-1/2}$ which is scaling found in past studies (Conde-Frias et al., 2023). The bed shear stress $\tau_b \sim \rho\nu\partial_z u|_{z=0}$ is given by

$$\frac{\tau_b}{\rho u_V^2} \sim \frac{C_D}{2}\sqrt{\frac{a_V d_V}{\mathrm{Re}_V^T(1-\phi_V)}} = \frac{C_D}{2\mathrm{Re}_V^T}\frac{d_V}{\delta_\nu}, \tag{S10}$$

where $C_D = C_D(u_V)$ is given by equation S1. If u_V represents the depth-averaged velocity U, this suggests that the bed friction $C_f = \tau_b/\rho U^2$ increases with vegetation density as the viscous sublayer thickness δ_ν decreases. The ratio between the vegetated bed shear stress τ_b compared to the shear stress without vegetation $\rho u_*^2 = \rho g h|\partial_x\eta|$ is

$$\frac{\tau_b}{\rho u_*^2} \sim \frac{C_D}{C_\infty}\left(\frac{u_V}{U_V}\right)^2 \frac{\delta_V}{h} \sim \frac{\delta_V}{h}, \tag{S11}$$

where the last relation assumes the turbulent limit with $C_D \sim C_\infty$ and $u_V \sim U_V$. This relation suggests that the bed shear stress is reduced by at least an order of magnitude

in the presence of dense vegetation $\delta_\nu \lesssim d_V \ll h$. This approximation for the bed shear stress (eq. S10, S11) is only accurate for smooth flows with a viscous sublayer (small bed-roughness/grain-sizes) and for a relatively small viscous boundary layers/stem diameters $\delta_\nu \lesssim d_V \ll h_V$ or $\phi_V \gtrsim 0.01,\ n_V \gtrsim 100\ \mathrm{m}^{-2},\ a_V \gtrsim 1\ \mathrm{m}^{-1}$.

The bed shear stress approximation above (eq. S10, S11) is found to be in agreement with flume experiments of Widdows, Pope, and Brinsley (2008) for a range of vegetation densities with real plant morphologies, *Spartina anglica*—a common marsh grass (Fig. S2). We also compare depth-averaged flow velocity measurements U to predictions u_V from equation S2 (Fig. S2a inset). From the flume experiments of Widdows et al. (2008), Figure S2a suggest that vegetation reduces the bed shear stress by almost two orders of magnitude compared to the vegetation free stress $\tau_b/\rho u_*^2 \sim \delta_\nu/h \ll 1$. This suggests we may ignore erosion effects on a tidal marsh platforms for the bulk of the tidal period. More work needs to be done to study the possibility of erosion at the beginning and end of the flood periods when depths are small.

S2. Suspended Sediment Transport Through Vegetation

Here we derive results for suspended sediment transport through marsh vegetation given the simplified flow dynamics outline above.

S2.1. Suspended Sediment Profiles for Low Rouse Numbers

Here we derive a general approximation for concentration profiles $\phi(z)$ and resulting ratios Φ/ϕ_0 for conditions where turbulent mixing is larger than grain settling (low Rouse number regime). From conservation of sediment (equation (5) in the main text) the

vertical flux of suspended sediment is given by

$$\varphi = (w - w_s)\phi - \nu_s \partial_z \phi.$$

At the water surface $z = h$ the flux is $\varphi(h) = w(h)\phi(h)$ giving the condition

$$\partial_z \phi = -\frac{w_s}{\nu_s}\phi \quad \text{at} \quad z = h.$$

On marshes we often assume pure deposition at the bed $\varphi(0) = -w_s\phi(0)$. However here we will assume the addition of a general erosion rate $\varphi(0) = -w_s\phi_0 + \varphi_\uparrow$. This gives the bed boundary condition

$$\partial_z \phi = -\frac{\varphi_\uparrow}{\nu_s} \quad \text{at} \quad z = 0.$$

For cases of nearly homogeneous, (quasi-) steady concentration profiles, we can expand $\phi(z)$ as

$$\phi(z)/\phi_0 \sim 1 - \alpha_1(z/h) - \alpha_2(z/h)^2,$$

where from the boundary conditions

$$\alpha_1 = \mathrm{Ro}\frac{\varphi_\uparrow}{w_s\phi_0} \quad \text{and} \quad \alpha_2 = \frac{\mathrm{Ro}/2}{1 + \mathrm{Ro}/2}\left[1 - (\mathrm{Ro} + 1)\frac{\varphi_\uparrow}{w_s\phi_0}\right],$$

where $\mathrm{Ro} = w_s h/\nu_s$ is the Rouse number. The depth average concentration $\Phi = \frac{1}{h}\int_0^h \phi(z)\mathrm{d}z$ is then approximated by

$$\frac{\Phi}{\phi_0} \sim 1 - \frac{\mathrm{Ro}}{2}\frac{\varphi_\uparrow}{w_s\phi_0} - \frac{\mathrm{Ro}/6}{1 + \mathrm{Ro}/2}\left[1 - (\mathrm{Ro} + 1)\frac{\varphi_\uparrow}{w_s\phi_0}\right]. \tag{S12}$$

The accuracy of this profile expansion requires that $\phi(z) \sim \Phi$ and therefore a small Rouse number $\mathrm{Ro} \lesssim 1$. On marshes we assume deposition dominance $w_s\phi_0 \gg \varphi_\uparrow$ (Fig. S2) which reduces the approximation above to equation (8) in the main text.

In open channel flow, erosion balances deposition $\varphi(z) = 0$ and the plug-flow Rouse profile is given by $\phi/\phi_0 = \exp(-\mathrm{Ro} \cdot z/h)$, with the bed concentration given by $\phi_0 = \varphi_\uparrow/w_s$. This gives the approximation $\Phi/\phi_0 \sim 1 - \mathrm{Ro}/2 + (\mathrm{Ro}^2/6)/(1 + \mathrm{Ro}/2)$ from equation (S12). (Note that this approximation diverges slowly, $\sim -\mathrm{Ro}/6$ as $\mathrm{Ro} \to \infty$.) In this idealized case the true ratio is $\Phi/\phi_0 = \mathrm{Ro}^{-1}(1 - \exp(-\mathrm{Ro}))$ and for small Ro this expands to $\Phi/\phi_0 \sim 1 - \mathrm{Ro}/2 + \mathrm{Ro}^2/6$, which is in fact a worse approximation than the one estimated by equation (S12). (Note that this approximation diverges nonlinearly fast, $\sim \mathrm{Ro}^2/6$ as $\mathrm{Ro} \to \infty$.) This provides support that equation (S12) is a good tool to gauge general approximations for Φ/ϕ_0 in turbulent transport regimes where $\mathrm{Ro} \lesssim 1$. Additionally, for the plug-flow approximation for submerged vegetation (Claudin et al., 2011), the depth-averaged eddy viscosity tends to be much larger than in emergent canopies (eq. S8). This suggests that if $\Phi/\phi_0 \sim 1$ in emergent vegetation (Fig. 2d, S3), then the approximation is even better for submerged canopies.

S2.2. Depth Averaged Dynamics

In the well mixed limit where concentration profiles are effectivity homogeneous $\Phi \sim \phi_0$ the evolution of the depth average concentration is approximated as

$$h\partial_t\Phi + Q\partial_x\Phi \sim -w_s\Phi. \tag{S13}$$

In quasi-steady state (large fluxes or shallow water depths) the average concentration evolves as

$$\Phi \sim \Phi(0,t)\exp\left(-\int \frac{w_s}{Q(x)}\mathrm{d}x\right).$$

For constant flux $Q(x) = Q$ the deposition length scale $L_D = Q/w_s$ as reported by Claudin et al. (2011). Similarly, for slow flow rates the depth average concentration settles out of the water column as

$$\Phi \sim \Phi(x, t_0) \exp\left(- \int \frac{w_s}{h(t)} \mathrm{d}t \right).$$

And for constant flow depth $h(t) = h$ the deposition time scale $T_D = h/w_s$ as also reported by Claudin et al. (2011).

The general depth averaged concentration can be solved explicitly along characteristic curves

$$\frac{\mathrm{d}x}{\mathrm{d}t} = U(x, t)$$

such that

$$\frac{\Phi(x,t)}{\Phi(0,t_0)} \sim \exp\left(- \int_{t_0(x)}^{t} \frac{w_s}{h(t)} \mathrm{d}t \right) = \exp\left(- \int_0^{x(t)} \frac{w_s}{Q(x)} \mathrm{d}x \right)$$

where $\Phi(0, t_0)$ is the concentration at $x = 0$ and is a function of characteristic time $t_0(x)$ parameterized along characteristic curves $x(t; t_0)$. More explicit expressions are found once the flow rate U and depth h are know.

S2.3. Analytical Approximations for Suspended Sediment Distribution

As we have shown in Figure 2, we can assume quasi-steady/geometric tidal flow over a marsh with $\eta(x,t) = \eta(t) = \delta \cos(2\pi t/T)$ and $Q = L\partial_t \eta(1 - x/L)$. Here $t \in (t_0, t_f)$ with flood period $\tau = (t_f - t_0)/T = \pi^{-1} \arccos(Z/\delta)$. In the initial flood stage ($t \sim t_0$) when h is small and Q is large (small Rouse number), the general profiles are homogeneous $\phi \sim \Phi$ and thus the initial concentration is distributed across the platform as

$$\lim_{t \to t_0} \phi(z, x, t) \sim \Phi(x, t) \sim \Phi_0 \exp\left(- \int_0^x \frac{w_s}{Q(x, t_0)} \mathrm{d}x \right) = \Phi_0 \left(1 - \frac{x}{L} \right)^{w_s^+} \tag{S14}$$

where Φ_0 is the channel concentration, $Q(x,t_0) = \partial_t\eta_0(L-x)$ and $w_s^+ = w_s/\partial_t\eta_0$ where the initial flood rate for platform elevation at $Z = 0$ is $\partial_t\eta_0 = 2\pi\delta/T$. Because the drainage divide L likely obtains residual diffusive sediment concentration from stochastic fluctuations we can reasonably assume a more simple distribution of the form

$$\lim_{t\to t_0}\phi(z,x,t) \sim \Phi(x,t) \sim \Phi_0 \exp\Big(-w_s^+\frac{x}{L}\Big).$$

This distribution should in principle also be true towards the end of the flood period ($t \sim t_f$) when the flow is high and depths are small. However when the marsh is draining there is no more sediment input from the channels so the magnitude must decrease. If the concentration at the channel edge $\Phi(0,t)$ is Φ_0 for flood periods and $r(t)\Phi_0$ for ebb (where $r < 1$) then

$$\lim_{t\to t_f}\phi(z,x,t) \sim \Phi(x,t) \sim r(t)\Phi_0 \exp\Big(-w_s^+\frac{x}{L}\Big).$$

Because the initial and final stages of the flood period over a marsh provides high flow and mixing rates, the suspended sediment concentration profiles are relatively homogeneous and decaying away from the channel according to the deposition length L/w_s^+. And at high tide when the flow/mixing rates tend to vanish (Ro $\gg 1$), the homogenized concentration $\phi(z) \sim \Phi$ settles out of the water column at rate h/w_s. For tidal amplitude of order 1 m and grain settling rates of order 10^{-4} m/s the settling rate is of order 10^4 s. This is much longer that the slack tidal period (around 1 hr). Thus we may expect that over a flood period, suspended transport over a marsh can be described by $\phi(z) \sim \Phi$.

Because the generalized deposition length scale is given by $Q(x,t)/w_s$, in quasi-steady state, we can approximate the average deposition length over the flood period by aver-

aging the flux scale $\langle Q \rangle = 2L\delta/T$. Thus we may expect the deposition length to scale as $\langle Q \rangle / w_s$. This phenomenological argument suggests a possible approximation of the flood-time average concentration

$$\overline{\Phi} \propto \Phi_0 \exp(-x/L_D) \quad \text{where} \quad L_D = \langle Q \rangle / w_s = \beta L\delta/Tw_s, \tag{S15}$$

where $2 < \beta < 4$ (Fig. 2, S4).

S2.4. Analytical Solution for Suspended Sediment Distribution

Taking the first order approximation that $\phi(z, x, t) \simeq \Phi(x, t)$, equation (6) in the main text reduces to equation S13 and is solved analytically for water depths $h = \delta \cos(2\pi t/T)$ and flux $Q(x, t) = -2\pi(L\delta/T)\sin(2\pi t/T)(1-x/L)$ to give the depth average concentration

$$\frac{\Phi(x,t)}{\Phi(0,t)} = \left[\left(1 - \frac{x}{L}\right) \frac{1 - \sqrt{1-(h/\delta)^2}}{1 - \sqrt{1-(h/\delta)^2(1-x/L)^2}} \right]^{-w_s^+}$$

where $w_s^+ = w_s/(2\pi\delta/T)$ and the concentration at the channel edge is given by

$$\frac{\Phi(0,t)}{\Phi_0} = \left[\frac{1 - \partial_t h/(2\pi\delta/T)}{1 - \sqrt{1-(h/\delta)^2}} \right]^{-w_s^+},$$

where Φ_0 is the sediment source concentration within the channel. We note that $\Phi(x,t)/\Phi(0,t)$ is symmetric about high tide and the initial concentration $\Phi(x, t_0) \sim (1 - x/L)^{w_s^+} \sim \exp(-w_s^+ x/L)$ varies slowly between $t = t_0$ and $t = 0$. Thus the time averaged concentration $\overline{\Phi}$ is well approximated by the heuristic scaling of equation (S15) (see Fig. 2f). In Figure S3 we compare this analytical approximation to depth-integrated solutions of equation (5)for a range of setting rates w_s and vegetation mixing lengths λ. The key quantity we want to obtain is the time average suspended sediment concentration $\overline{\Phi}(x)$. Figure S3 shows that solutions for the approximation that $\Phi \sim \phi_0$ works reasonably

well for most cases and most importantly generally captures the scaling behavior of the decay of $\overline{\Phi}(x)$ away from the channel.

S3. Effects of Variable Marsh Platform Elevation

The results up until now have focused on flat marsh platforms $Z(x) = Z$. Solutions of Φ above have only been considered for platform surfaces at mean sea level $Z = 0$. Here we consider variations in platform slopes and elevations.

S3.1. Channel-bound Marshes

For marshes bounded by channels (the main focus of this study), bed elevations tend to decrease from the channel (e.g., Marani, Da Lio, and D'Alpaos (2013); Christiansen, Wiberg, and Milligan (2000)). We can approximate the small elevation changes as $Z(x) \sim Z_0 - (Z_0 - Z_L)x/L$ where the platform declines from $Z(0) = Z_0$ to $Z(L) = Z_L$ at the basin divide L.

The distribution of suspended sediment $\Phi(x)$ at the beginning of platform flood depends on the initial flux $Q_0 \sim L\partial_t h_0$ where $\partial_t h_0$ is the tidal rate at the initial flood time $t_0/T = -\tau/2$ where $\tau = \pi^{-1}\arccos(Z/\delta)$. Thus $\partial_t h_0 = 2\pi\sqrt{1-(Z/\delta)^2}$. The suspended sediment concentration initially decays with the deposition length $\sim L\partial_t h_0/w_s$, thus the average deposition length is approximated as

$$\frac{L_D}{L} \sim \beta\frac{\delta/T}{w_s}\sqrt{1-(Z/\delta)^2} \tag{S16}$$

where $\beta \sim 3$. Because variations in $Z(x)$ are minor over a marsh platform and elevations tend to fall closer to mean sea level, $\sqrt{1-(Z/\delta)^2} \sim 1$, the effects of variable $Z(x)$ of suspended sediment distributions over a channel-bound marsh are typically minor. In

Figure S3 we test that variable $Z(x)$ does not greatly alter the time-averaged approximation $\overline{\Phi}(x) \propto \exp(-x/L_D)$ for a wide range of settling rates $w_s/(\delta/T)$ and channel-bound marsh elevations $Z/\delta = [0, 1/2, (1 - x/L)/2]$.

S3.2. Upland Marshes

Some marshes (or marsh sections) emerge off an upland. At the marsh edge ($x = 0$) there is an upland slope S that gets flooded up to a distance $L = \delta/S$, for tidal amplitude δ. The water depths can be approximated as $h(x,t) = h_0(t) - Sx$ and the flux of water across the upland marsh is $Q(x,t) = h(x,t)\partial_t h(t)/S$—i.e., a spatially constant flow velocity $U(t) = \partial_t h(t)/S$. The characteristic solution to equation S13 for upland geometry is

$$\frac{\Phi(x,t)}{\Phi_0} = \exp\left[\frac{-w_s}{h(x,t)}(t - t_0(x,t))\right], \tag{S17}$$

with characteristic time $t_0(x,t) = -\frac{T}{2\pi}\arccos(h(x,t)/\delta)$.

The time-averaged concentration $\overline{\Phi}(x)$ depends on a deposition length scale that is about half as large as the flat channel-bound case (i.e., $\beta \sim 3/2$; Fig. S4). This can be thought of as taking the effective basin length as half the flood distance, $L_{\text{eff}} \sim L/2 = \delta/2S$.

References

Butzeck, C., Eschenbach, A., Gröngröft, A., Hansen, K., Nolte, S., & Jensen, K. (2015). Sediment deposition and accretion rates in tidal marshes are highly variable along estuarine salinity and flooding gradients. *Estuaries and Coasts*, *38*, 434–450.

Christiansen, T. (1998). *Sediment deposition on a tidal salt marsh.* University of Virginia.

Christiansen, T., Wiberg, P. L., & Milligan, T. (2000). Flow and sediment transport on a tidal salt marsh surface. *Estuarine, Coastal and Shelf Science*, *50*(3), 315–331.

Claudin, P., Charru, F., & Andreotti, B. (2011). Transport relaxation time and length scales in turbulent suspensions. *Journal of Fluid Mechanics*, *671*, 491–506.

Coleman, D. J., Ganju, N. K., & Kirwan, M. L. (2020). Sediment delivery to a tidal marsh platform is minimized by source decoupling and flux convergence. *Journal of Geophysical Research: Earth Surface*, *125*(8), e2020JF005558.

Coleman, D. J., & Kirwan, M. L. (2019). The effect of a small vegetation dieback event on salt marsh sediment transport. *Earth Surface Processes and Landforms*, *44*(4), 944–952.

Conde-Frias, M., Ghisalberti, M., Lowe, R., Abdolahpour, M., & Etminan, V. (2023). The near-bed flow structure and bed shear stresses within emergent vegetation. *Water Resources Research*, *59*(4), e2022WR032499.

Duran Vinent, O., Herbert, E. R., Coleman, D. J., Himmelstein, J. D., & Kirwan, M. L. (2021). Onset of runaway fragmentation of salt marshes. *One Earth*, *4*(4), 506–516.

Etminan, V., Ghisalberti, M., & Lowe, R. J. (2018). Predicting bed shear stresses in vegetated channels. *Water Resources Research*, *54*(11), 9187–9206.

French, J. R., & Spencer, T. (1993). Dynamics of sedimentation in a tide-dominated backbarrier salt marsh, norfolk, uk. *Marine Geology*, *110*(3-4), 315–331.

King, A., Tinoco, R., & Cowen, E. (2012). A k–ε turbulence model based on the scales of vertical shear and stem wakes valid for emergent and submerged vegetated flows. *Journal of Fluid Mechanics*, *701*, 1–39.

Leonard, L. A., & Croft, A. L. (2006). The effect of standing biomass on flow velocity and turbulence in spartina alterniflora canopies. *Estuarine, Coastal and Shelf Science*,

69(3-4), 325–336.

Li, H., & Yang, S. (2009). Trapping effect of tidal marsh vegetation on suspended sediment, yangtze delta. *Journal of coastal research*, *25*(4), 915–924.

Liu, C., Shan, Y., He, L., Li, F., Liu, X., & Nepf, H. (2024). Plant morphology impacts bedload sediment transport. *Geophysical Research Letters*, *51*(12), e2024GL108800.

Marani, M., Da Lio, C., & D'Alpaos, A. (2013). Vegetation engineers marsh morphology through multiple competing stable states. *Proceedings of the National Academy of Sciences*, *110*(9), 3259–3263.

Reed, D. J., Spencer, T., Murray, A. L., French, J. R., & Leonard, L. (1999). Marsh surface sediment deposition and the role of tidal creeks: implications for created and managed coastal marshes. *Journal of Coastal conservation*, *5*, 81–90.

Stumpf, R. P. (1983). The process of sedimentation on the surface of a salt marsh. *Estuarine, Coastal and Shelf Science*, *17*(5), 495–508.

Tanino, Y., & Nepf, H. M. (2008a). Laboratory investigation of mean drag in a random array of rigid, emergent cylinders. *Journal of Hydraulic Engineering*, *134*(1), 34–41.

Tanino, Y., & Nepf, H. M. (2008b). Lateral dispersion in random cylinder arrays at high reynolds number. *Journal of Fluid Mechanics*, *600*, 339–371.

Temmerman, S., Govers, G., Wartel, S., & Meire, P. (2003). Spatial and temporal factors controlling short-term sedimentation in a salt and freshwater tidal marsh, scheldt estuary, belgium, sw netherlands. *Earth Surface Processes and Landforms: The Journal of the British Geomorphological Research Group*, *28*(7), 739–755.

van Proosdij, D., Davidson-Arnott, R. G., & Ollerhead, J. (2006). Controls on spatial

patterns of sediment deposition across a macro-tidal salt marsh surface over single tidal cycles. *Estuarine, Coastal and Shelf Science*, *69*(1-2), 64–86.

Wang, F. C., Lu, T., & Sikora, W. B. (1993). Intertidal marsh suspended sediment transport processes, terrebonne bay, louisiana, usa. *Journal of Coastal Research*, 209–220.

Widdows, J., Pope, N. D., & Brinsley, M. D. (2008). Effect of spartina anglica stems on near-bed hydrodynamics, sediment erodability and morphological changes on an intertidal mudflat. *Marine Ecology Progress Series*, *362*, 45–57.

Yang, J. Q., Kerger, F., & Nepf, H. M. (2015). Estimation of the bed shear stress in vegetated and bare channels with smooth beds. *Water Resources Research*, *51*(5), 3647–3663.

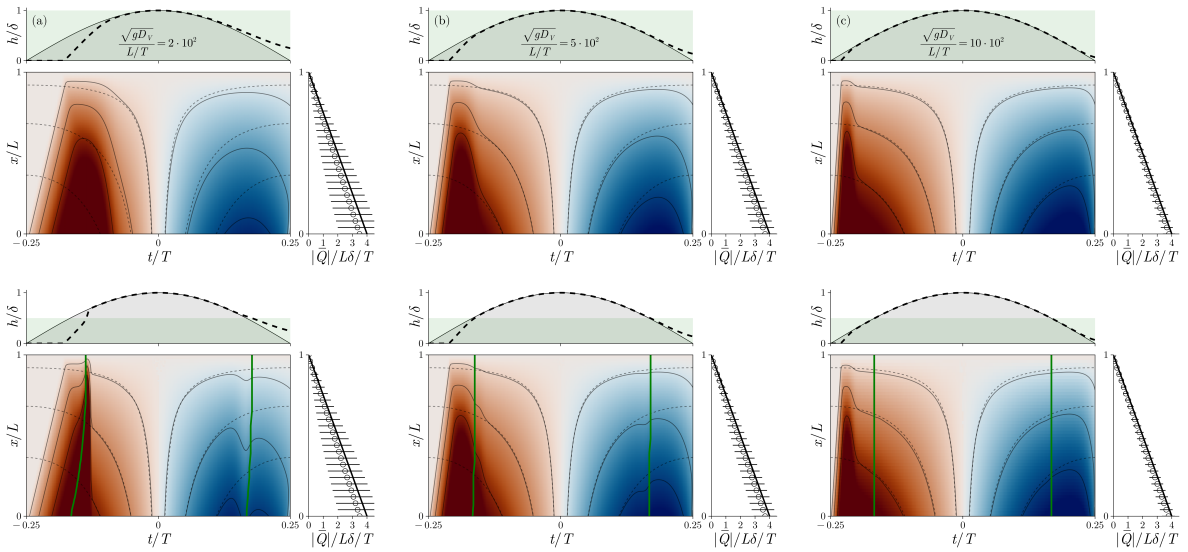

Figure S1. Numerical solutions of the flow over a densely vegetated marsh platform solving $\partial_t h = -\partial_x(hU)$. For each panel the top plot shows tidal amplitude in the channel $h(0,t) = \delta\cos(2\pi t/T)$ (gray shaded region) and at the basin divide $h(L,t)$ (dashed line)—green shaded region is the vegetation reference height h_V. The contour plot shows the flux $Q/(L\delta/T)$ with colors ranging from $(-5,5)$ and black contours at $(\pm 0.5, \pm 2, \pm 4)$—dashed contours are the geometric approximation $Q_0 \sim (L-x)\partial_t h(0,t)$. Right plot shows time average of the flux magnitude $|\overline{Q}|$ for simulated flow (markers) with bars being average deviations $|\overline{Q-Q_0}|$—solid line is the approximation $|\overline{Q}_0| \sim 4(L-x)\delta/T$. Top row of panels is for vegetation heights larger than the tidal amplitude $h_V > \delta$ using $U = U_V$ (eq. S3) and bottom row is for vegetation heights $h_V = \delta/2$ using $U = U_V$ for $h(x,t) < h_V$ and then equation S6 for $h(x,t) > h_V$. Parameters are: column (a) $\sqrt{gD_V}/(\delta/T) = 2 \cdot 10^4,\ L/\delta = 100$; column (b) $\sqrt{gD_V}/(\delta/T) = 5 \cdot 10^4,\ L/\delta = 100$; column (c) $\sqrt{gD_V}/(\delta/T) = 5 \cdot 10^4,\ L/\delta = 50$. Column (a) represents extremely dense vegetation $a_V \sim 50\ \mathrm{m}^{-1},\ n_V \sim 5000\ \mathrm{m}^{-2},\ \phi_V \sim 0.5$ where as columns (b,c) are more realistic marsh densities $a_V \sim 8\ \mathrm{m}^{-1},\ n_V \sim 800\ \mathrm{m}^{-2},\ \phi_V \sim 0.08$. In the bottom row of panels the green lines show when $h(x,t) = h_V$. Note that for lower vegetation densities or for smaller basin lengths (i.e., larger $\sqrt{gD_V}/(L/T)$) than what is shown, the approximation $Q(x,t) \sim Q_0(x,t)$ becomes more accurate.

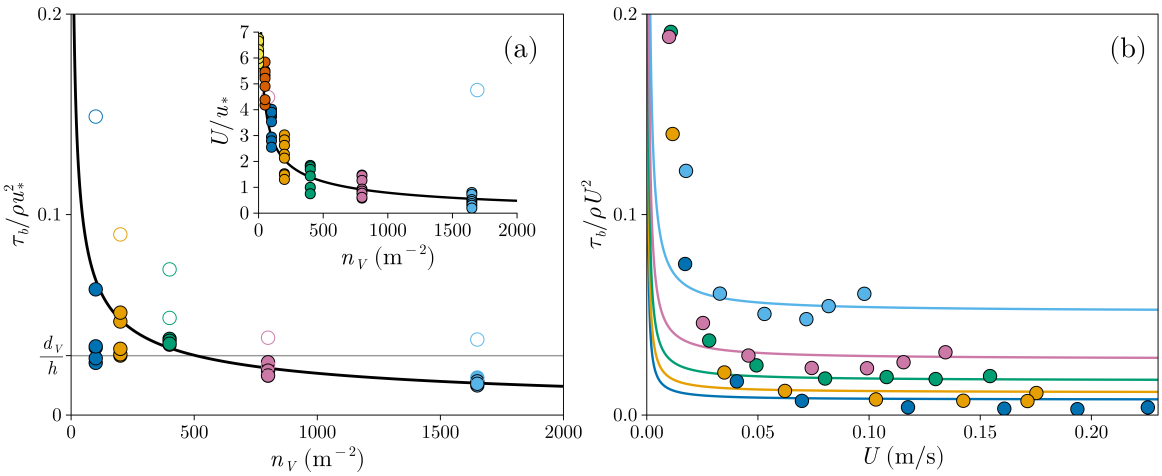

Figure S2. Experimental measurements of vegetated bed shear stress compared with predictions. (a) Vegetated bed shear stress τ_b relative to the vegetation free bed shear stress ρu_*^2 versus vegetation density n_V. Inset in (a) shows average flow velocity versus vegetation density. (b) The bed friction coefficient $C_f = \tau_b/\rho U^2$. In (a) experimental data shown as filled markers represent the turbulent regime for $U > 0.05$ m/s ($\mathrm{Re}_V \gtrsim 400$, $\mathcal{R} \gtrsim 20$) and open markers are $U < 0.05$ m/s ($\mathrm{Re}_V \lesssim 400$, $\mathcal{R} \lesssim 20$). Black line is the turbulent prediction $\tau_b/\rho u_*^2 \sim \delta_\nu/h$ (eq. S11)—which is independent of the flow velocity. Grey line shows $d_V/h \sim 0.03$ using approximate stem diameter $d_V = 0.8$ cm and reported flow depth $h = 27$ cm. Inset in (a) shows measurements of U/u_* from the same experiments versus stem density n_V. Black line is the approximation $u_V/u_* \propto 1/\sqrt{a_V h}$ (eq. S2) using $u_* = \sqrt{gh|\partial_x \eta|}$. Panel (b) shows the vegetated bed friction coefficient $\tau_b/\rho U^2$ with predictions from equation S10. Colors correspond to different vegetation densities in (a). All data (markers) are flume experiments of Widdows et al. (2008) using plant species *Spartina anglica* at densities $n_V = 100$ m^{-2} (dark blue), $n_V = 200$ m^{-2} (orange), $n_V = 400$ m^{-2} (green), $n_V = 800$ m^{-2} (pink), $n_V = 1650$ m^{-2} (light blue). Widdows et al. (2008) do not report u_*, they only report annular flume rotations per minute ω. We approximate the constant ratio u_*/ω from the depth averaged flow velocity for zero stems $n_V = 0$, which takes the form $U/u_* \sim \kappa^{-1}(\log(h/d_V) - 1)$ where we assume bed roughness is set by d_V. We find $u_*/r\omega = 0.1 \pm 0.005$ where $r = 44$ cm is the flumes inner radius. All predictions (eq. S10, S11, S2) use stem diameter $d_V = 0.8$ cm, reported flow depth $h = 27$ cm, and drag coefficients values $\mathrm{Re}_V^T \sim 30$ and $C_\infty \sim 1 + 8\phi_V$ (Tanino & Nepf, 2008a).

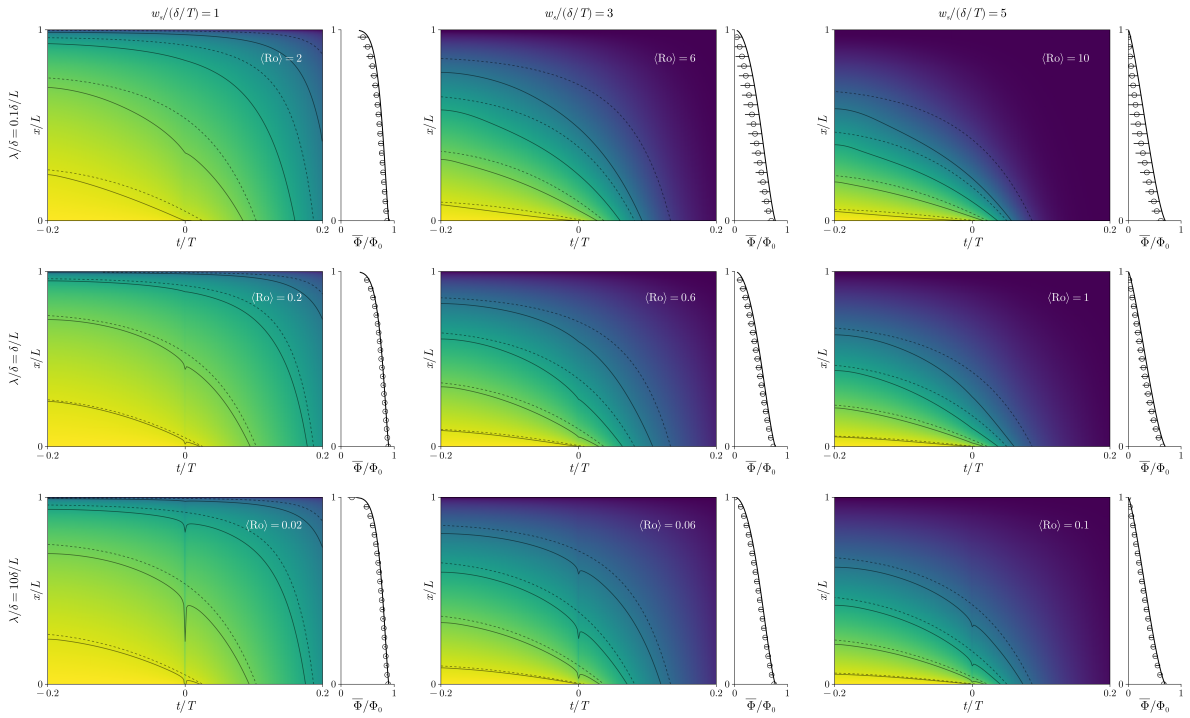

Figure S3. Numerical solutions of depth averaged suspended sediment concentrations over a flat marsh with emergent vegetation solving equation (5) in the main text, using geometric $Q(x,t)$ and eddy viscosity $\nu_t(x,t) = \lambda|U|$ from equations (1) and (4) in the main text. Contour plots show ratio $\Phi(x,t)/\Phi_0$ with colors ranging from (0,1) and black contour lines (0.4, 0.6, 0.8, 0.95)—dashed contours are using the approximation of well-mixed, homogeneous profiles $\Phi = \phi_0$ (eq. S13, S14). Right panels are time averages $\overline{\Phi}(x)/\Phi_0$ from numerical solutions (markers) and well-mixed approximations (line) with bars being average deviations from well-mixed approximation. Rows are varying the vegetation mixing length parameter $\lambda L/\delta^2$ and columns are varying grain setting rates $w_s/(\delta/T)$. Also shown are the average Rouse numbers $\langle \mathrm{Ro} \rangle = \frac{2}{\pi^2}\frac{w_s\delta}{\lambda L/T}$. Because $\lambda \sim \mathcal{O}(d_V)$, the values of $\lambda L/\delta^2 = (0.1, 1, 10)$ represent $d_V \sim \mathcal{O}(0.1, 1, 10)$ cm. Note that typical values are $d_V = 1$ cm.

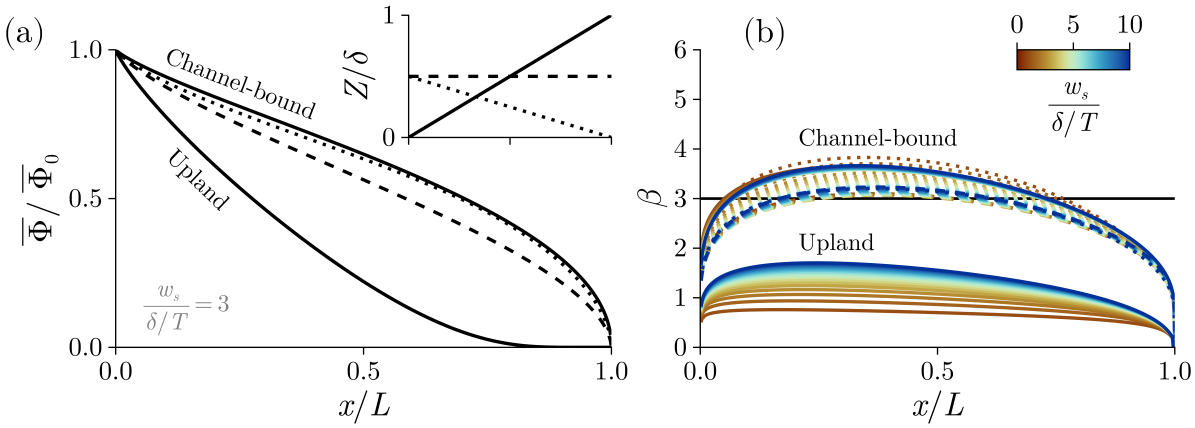

Figure S4. Platform elevation effects on the time averaged suspended sediment concentration. (a) Time averaged concentration $\overline{\Phi}$ normalized by the average channel value $\overline{\Phi}_0 = \overline{\Phi}(0,t)$ for channel-bound and upland marshes. Bed elevation variations $Z(x)$ are shown in the inset. For channel-bound marshes, $Z/\delta = 0$ (solid line), $Z/\delta = 1/2$ (dashed line), $Z/\delta = (1 - x/L)/2$ (dotted line). For upland geometry, $Z/\delta = x/L$ where $L = \delta/S$. (b) Distributions of β from equation S16 for $L_D = x/\log\left(\overline{\Phi}_0/\overline{\Phi}\right)$ for various solutions of $\overline{\Phi}(x)$ for a range of $w_s/(\delta/T)$ and bed elevations (line styles correspond to panel a). Average values of β for channel-bound marshes are around $\beta \sim 3$ for all bed geometries and settling rates. For upland solutions, $1 \lesssim \beta \lesssim 3/2$ for the range of $w_s/(\delta/T)$ and approaches $\beta \sim 3/2$ for $w_s/(\delta/T) \gg 0$.

Table S1. Summary of parameters and variables.

Geometry		
$x \in (0, L)$	Distance from channel to basin divide, L (i.e., the center point between two channels)	$L \sim$ 10–100 m (occasionally $>$ 100 m)
δ, T	Tidal amplitude and period	$\delta \sim$ 0.5–1.5 m (up to $\sim$ 5 m macro-tidal), $T \sim$ 12.5 hr (semi-diurnal)–24 hr (diurnal)
$\eta(x,t)$	Water surface elevation over the platform; well approximated by water elevation in channel, $\eta(x,t) \simeq \eta_0(t)$	Order δ
$h(x,t)$	Local water depth over platform, $h(x,t) = \eta(x,t) - Z(x)$	Order δ
$Z(x)$	Platform elevation (fixed on time scales of order T)	Taken to be $Z \sim 0$ m above sea level; See Section 3 for results with variable $Z(x)$
Vegetation		
a_V	Vegetation frontal area per unit volume	1–10 m^{-1} (dense up to $\sim$ 50 m^{-1})
n_V	Stem density (stems per unit area)	10^2–10^3 m^{-2}
d_V	Effective stem diameter, $d_V = a_V/n_V$	Order 1 cm
ϕ_V	Vegetation volume fraction $\phi_V \sim a_V d_V$	0.01–0.1
D_V	Vegetation drag length, $D_V \sim 1/a_V$ (see Section S1.1 for more details)	0.1–1 m
Flow		
$Q(x,t)$	Volumetric flux per unit width—well approximated by geometric flux, $Q \sim \partial_t \eta_0 (L - x)$	10^{-3}–10^{-2} m^2/s
$U(x,t)$	Depth-averaged velocity, $U = Q/h$	10^{-3}–10^{-1} m/s
u_V	Vegetation-limited characteristic velocity, $u_V \sim \sqrt{g D_V \lvert\partial_x \eta\rvert}$	Order U
k_V	Vegetation-generated turbulent kinetic energy, $\sqrt{k_V}/u_V \sim (d_V/D_V)^{1/3} \sim \phi_V^{1/3}$	$\sqrt{k_V} \sim 10^{-4}$–10^{-2} m/s
ν_t	Eddy viscosity—in vegetated canopies given by $\nu_t \sim d_V \sqrt{k_V} \sim \lambda \lvert U \rvert$	10^{-5}–10^{-3} m^2/s
λ	Mixing length (wake) scale, $\lambda \sim d_V \phi_V^{1/3}$	10^{-3}–10^{-2} m
Sediment		
w_s	Grain settling velocity	Order 10^{-4} m/s

ν_s	Sediment diffusivity	Approximated as $\nu_s \simeq \nu_t$
Ro	Rouse number (settling to mixing rate ratio), $\mathrm{Ro} = w_s h/\nu_s$	$0.1 \lesssim \mathrm{Ro} < 10$
$\langle \mathrm{Ro} \rangle$	Marsh average Rouse number, $\langle \mathrm{Ro} \rangle = w_s \langle h \rangle / \lambda \langle U \rangle$ for $\langle h \rangle = 2\delta/\pi$ and $\langle U \rangle = \langle Q \rangle / \langle h \rangle$ with $\langle Q \rangle = 2\delta L/T$	$0.1 \lesssim \langle \mathrm{Ro} \rangle < 10$
$\phi(z, x, t)$	Local suspended sediment concentration	
Φ_0	Channel concentration	10–100 mg/L (site specific)
$\Phi(x, t)$	Depth-averaged concentration	$\lesssim \Phi_0$
$\phi_0(x, t)$	Near-bed concentration, $\phi(z = 0) \sim \Phi$ (for low Ro)	$\lesssim \Phi_0$
$\overline{\Phi}$	Tidal (flood-period) average concentration—well approximated as $\overline{\Phi} \sim \overline{\Phi}_0 \, e^{-x/L_D}$	$\lesssim \Phi_0$
$\overline{\Phi}_0$	Tidal (flood-period) average concentration at marsh edge $\overline{\Phi}_0 = \overline{\Phi}(x = 0)$,	$\lesssim \Phi_0$
L_D	Deposition decay length, $L_D = \beta L(\delta/T)/w_s$	0.1–1 $L \sim$ 1–10^2 m (site specific)
β	Coefficient in L_D scaling	2–3

Table S2. Data parameters used in Figure 3in the main text. We assume the typical value $w_s \sim 10^{-4}$ m/s if settling rates (or grain sizes) were not reported (Duran Vinent et al., 2021). Basin sizes are approximated by the distance between channels from published marsh maps, or if that cannot be done L is the maximum distance reported (Duran Vinent et al., 2021). For marshes with increasing elevations away from channels L is taken as half the maximum flood length—approximating the average basin length over a flood period (see Fig S4). Because L and w_s are the most uncertain parameters, we expect errors of around ±50%.

Location	**Vegetation**	$\boldsymbol{\delta}$	$\boldsymbol{T}$	$\boldsymbol{w_s}$	$\boldsymbol{L}$
Phillips Creek, VA, US (Christiansen, 1998)	*Spartina alterniflora*; $0.5 \lesssim h_V \lesssim 1$ m; $100 \lesssim n_V \lesssim 200$ m^{-2}	1 m	12.5 hr	$w_s \sim 10^{-4}$ m/s: Based on typical grain size of $\sim$ 10 μm (Christiansen et al., 2000).	$L \sim 50$ m: Based on marsh platform map.
Altamaha River Estuary, GA, US (Coleman & Kirwan, 2019)	*Spartina alterniflora*; Biomass $\sim$ 1 kg/m^2	1.15 m	12.5 hr	$w_s \sim 10^{-4}$ m/s	$L \sim 20$ m: Based on maximum distance reported and marsh platform map.
Plum Island Estuary, MA, US (Coleman et al., 2020)	*Spartina alterniflora/patens*; $100 \lesssim$ Biomass $\lesssim 600$ g/m^2	1.5 m	12.5 hr	$w_s \sim 10^{-4}$ m/s	$L \sim 25$ m: Based on maximum distance reported and marsh platform map.
Hut Marsh, Norfolk, UK (French & Spencer, 1993)	Mixed species; Biomass $\sim \mathcal{O}(100)$ g/m^2	3.5 m	12.5 hr	$w_s \sim 3 \cdot 10^{-4}$ m/s for 5 year mean and $w_s \sim 5.5 \cdot 10^{-4}$ m/s for individual tides (Duran Vinent et al., 2021)	$L \sim 200$ m: Based on maximum distance reported.

Allen Creek, Bay of Fundy, Canada (van Proosdij et al., 2006)	*Spartina patens* (high marsh) and *Spartina alterniflora* (low marsh); $h_V \sim 0.25$ m	5.5 m	12.5 hr	$w_s \sim 10^{-4}$ m/s (Duran Vinent et al., 2021)	$L \sim 160$ m: Based on maximum distance reported.
Elbe Estuary, Germany (Butzeck et al., 2015)	Mixed species; Biomass ~ 600 g/m^2	1.5 m	12.5 hr	$w_s \sim 3 \cdot 10^{-4}$ m/s from minimum grain size measurable by the laser diffraction sensor.	From marsh maps: TFM – Near creek $L \sim 100$ m; Marsh edge $L \sim 200$ m half flood distance. BM – Near creek $L \sim 100$ m; Marsh edge $L \sim 400$ m half flood distance. SM – Near creek $L \sim 30$ m; Marsh edge $L \sim 500$ m half flood distance.
Hut Marsh, Norfolk, UK (Reed et al., 1999)	*Atriplex portulacoides*; $h_V \sim 0.25$ m	3.5 m	12.5 hr	$w_s \sim 5.5 \cdot 10^{-4}$ m/s as for individual tides for French and Spencer (1993) (Duran Vinent et al., 2021)	$L \sim 20$ m: Based on maximum distance reported.
Terrebonne Bay, LA, US (Wang et al., 1993)	*Spartina alterniflora*; vegetated area per m^2 $\sim$ 50%	0.5 m	24 hr	$w_s \sim 10^{-4}$ m/s	$L \sim 350$ m: Based on maximum distance reported.
Scheldt estuary, Belgium/Netherlands (Temmerman et al., 2003) (Data used from Fig. 7b)	Mixed species; $h_V \sim 0.5$ m; $50 \lesssim n_V \lesssim 500$ m^{-2}	Typical value $\delta \sim 2$ m	12.5 hr	$w_s \sim 10^{-4}$ m/s	$L \sim 40$ m: Based on marsh maps.
Southeastern North Carolina Marshes, US (Leonard & Croft, 2006)	*Spartina alterniflora*; $0.1 \lesssim h_V \lesssim 1$ m; $150 \lesssim n_V \lesssim 300$ m^{-2}	1.5 m	12.5 hr	$w_s \sim 10^{-4}$ m/s	$L \sim 20$ m: Based on maximum distance reported.

Holland Glade Marsh, DE, US (Stumpf, 1983)	*Spartina alterniflora*; $0.1 \lesssim h_V \lesssim 1$ m; $n_V \sim 450$ m^{-2}	0.5 m	12.5 hr	$w_s \sim 10^{-4}$ m/s	$L \sim 20$ m: Based on maximum distance reported and marsh map.
Yangtze delta, Shanghai (Li & Yang, 2009)	Mixed species; $0.5 \lesssim h_V \lesssim 2$ m; $1 \lesssim$ Biomass $\lesssim 5$ kg/m^2	1.5 m	12.5 hr	$w_s \sim 10^{-4}$ m/s	$L \sim 50$ m: Based on maximum distance reported.